The Astrophysical Journal, 982:30 (16pp), 2025 March 20 https://doi.org/10.3847/1538-4357/ad8b4b

Relight the Candle: What Happens to High-redshift Massive Quenched Galaxies

Rhea-Silvia Remus and Lucas C. Kimmig
Universitäts-Sternwarte München, Fakultät für Physik, Ludwig-Maximilians Universität, Scheinerstr. 1, D-81679 München, Germany; rhea@usm.lmu.de
Received 2023 October 24; revised 2024 October 20; accepted 2024 October 23; published 2025 March 12

Abstract

A puzzling population of extremely massive quiescent galaxies at redshifts beyond $z = 3$ has recently been revealed by JWST and the Atacama Large Millimeter/submillimeter Array, some of them with stellar ages that show their quenching times to be as high as $z = 6$, while their stellar masses are already above $5 \times 10^{10}\ M_{\odot}$. These extremely massive yet quenched galaxies challenge our understanding of galaxy formation at the earliest stages. Using the hydrodynamical cosmological simulation suite Magneticum Pathfinder, we show that such massive quenched galaxies at high redshifts can be successfully reproduced with similar number densities as observed. The stellar masses, sizes, formation redshifts, and star formation histories of the simulated quenched galaxies match those determined with JWST. Following these quenched galaxies at $z = 3.4$ forward in time, we find 20% to be accreted onto a more massive structure by $z = 2$, and from the remaining 80% about 30% rejuvenate up to $z = 2$, another 30% stay quenched, and the remaining 40% rejuvenate on a very low level of star formation. Stars formed through rejuvenation are mostly formed on the outer regions of the galaxies, not in the centers. Furthermore, we demonstrate that the massive quenched galaxies do not reside in the most massive nodes of the cosmic web, but rather live in side nodes of approximately Milky Way halo mass. Even at $z = 0$, only about 10% end up in small-mass galaxy clusters, while most of the quenched galaxies at $z = 3.4$ end up in group-mass halos, with about 20% actually not even reaching $10^{13}\ M_{\odot}$ in halo mass.

Unified Astronomy Thesaurus concepts: Galaxies (573); High-redshift galaxies (734); Galaxy evolution (594); Quenched galaxies (2016); Computational methods (1965)

1. Introduction

The high-redshift Universe has become available to observations in the last year thanks to JWST in unprecedented detail, revealing star-forming galaxies to exist at redshifts as high as $z = 13$ or possibly higher from photometry (e.g., N. J. Adams et al. 2023; Y. Harikane et al. 2023), and despite some of them having shown to be at lower redshifts by spectroscopic follow-up, several of them have been confirmed at redshifts as high as $z = 13$ (e.g., P. Arrabal Haro et al. 2023; Y. Harikane et al. 2024). Furthermore, the Atacama Large Millimeter/submillimeter Array has added to the zoo of high-redshift galaxies observations of low-turbulence but dust-obscured disk galaxies that cannot be detected by JWST due to their high dust content (e.g., F. Lelli et al. 2023; F. Rizzo et al. 2023). Such dust-obscured galaxies with average star formation rates have been found even up to $z = 7$ (Y. Fudamoto et al. 2021). Massive galaxies with disk morphologies have been resolved at redshifts up to at least $z = 4$ (e.g., T. Tsukui & S. Iguchi 2021; F. Roman-Oliveira et al. 2023), with star formation rates of more than 1000 $M_{\odot}\ \mathrm{yr}^{-1}$ and strong active galactic nucleus (AGN) activity (T. Tsukui et al. 2023), but also some spiral galaxies have been reported at those redshifts that show signs of their star formation being shut off (Y. Fudamoto et al. 2022; E. J. Nelson et al. 2023). All of these observations challenge our understanding of galaxy formation and the overall structure formation and cosmology when the Universe was very young, and are the perfect test bed for theoretical models and simulations to probe our grasp on the underlying physics.

To this zoo of extraordinary galaxies at high redshift also belong massive quenched galaxies, that is, galaxies at redshifts as high as $z = 4$ with stellar masses of $M_{*} > 3 \times 10^{11}\ M_{\odot}$ (C. Schreiber et al. 2018; T. Nanayakkara et al. 2022; A. C. Carnall et al. 2023; A. S. Long et al. 2024), for which spectroscopically their formation times, i.e., the time at which half of their stars have been formed, were confirmed to be as high as $z = 6$–7 (T. Nanayakkara et al. 2022; A. C. Carnall et al. 2023), in one case even as high as $z = 11$ (K. Glazebrook et al. 2023). These quiescent galaxies are found in significant numbers at high redshift, unexpectedly, with the overall gas content in these galaxies being much higher than at present day; thus, it is still a matter of debate how these galaxies have come to be quenched at such early times, how they evolve after they were quenched, and what they become at $z = 0$.

Quenched, or quiescent, galaxies at high redshifts are known to be more compact than their present-day counterparts of the same stellar mass, more so the higher the redshift (e.g., A. van der Wel et al. 2014; K. Ito et al. 2024). Such compact quiescent galaxies are not observed at low redshifts, at least not in quantities that can account for the numbers of compact quenched galaxies now reported for high redshifts. Multiple dry minor mergers have been proposed as a possible formation pathway for such quenched galaxies (F. Bournaud et al. 2007; R. Bezanson et al. 2009; T. Naab et al. 2009), as such small mergers deposit most of their stellar mass at larger radii and as such enhance the radial growth compared to normal major merger events (M. Hilz et al. 2012; G. S. Karademir et al. 2019). However, dry mergers are known to be more common the lower the redshift (e.g., E. F. Bell et al. 2006), and rather rare at high redshifts before $z = 2$, where the gas fractions are generally much higher. Thus, other additional evolution pathways for such high-redshift quenched galaxies are required. One possible evolution pathway is for the compact

quenched galaxy to merge into another, more massive (and possibly still star forming) galaxy as the minor progenitor.

Another suggested pathway is so-called rejuvenation, that is, reaccretion of gas from either the cosmic web or through gas-rich mergers onto the central galaxy, thereby reforming a disk and restarting star formation. Indications for such a process have been found imprinted in observed quiescent galaxies at present day (e.g., S. K. Yi et al. 2005), clearly showing that the simple assumption that once a galaxy has been quenched it stays quenched is not valid. Similarly, about 16% of the quiescent galaxies found at $z \approx 0.8$ in the LEGA-C survey show signs of rejuvenation (P. Chauke et al. 2019). Models predict a range of 10%–70% of all massive galaxies to have lived through a rejuvenation phase (J. Zhang et al. 2023), and even the possibility of multiple rejuvenation events for a galaxy throughout its life (T. S. Tanaka et al. 2024). The exact conditions under which some quenched galaxies can revive through accretion of new gas and others do not are yet not well understood. However, observations of local galaxies that host AGN show signs that their last massive starburst event occurred at the same time as the last AGN activity, indicating that both AGN activity and the massive starburst might have been triggered by the same event (I. Martin-Navarro et al. 2022).

Using the Illustris-TNG300 simulation, A. I. Hartley et al. (2023) identified five quenched galaxies emerging at $z = 4.2$, which were all quenched by the implemented AGN feedback and ended up as the most massive nodes of the box at $z = 0$. However, their predicted number densities of quenched galaxies is significantly lower[1] than what has been observed by A. C. Carnall et al. (2023) and A. S. Long et al. (2024). More problematic, observations also report some of the quenched galaxies to have been quenched since $z = 5$ or earlier (T. Nanayakkara et al. 2022; A. C. Carnall et al. 2023), which is higher than found for any quenched galaxy in that simulation (T. Kakimoto et al. 2024). Thus, many questions are actually still open, which we will address in this study together with its companion study by L. C. Kimmig et al. (2025, hereafter K25).

This paper will focus on the properties and future evolution pathways of quenched galaxies found in the Magneticum simulations, and compare the properties of those galaxies to observations. The companion paper (K25) focuses on the mechanisms and environmental conditions that lead to the quenching, discussing how the feedback both from the stars and the central supermassive black hole combined is responsible. The paper is structures as follows: Section 2 will introduce the simulation suite used to study quenched galaxies at high redshifts. Section 3 presents the sample of quiescent galaxies, and compares global properties between quenched simulated and observed galaxies, including the formation redshifts obtained from stellar populations. Section 4 focuses on the different pathways galaxies follow after they have been quenched at high redshifts. In particular, we discuss the process of rejuvenation, with an outlook to the halo properties of the quenched galaxies at $z = 0$. Finally, Section 5 will summarize the results and discuss them in the global context of galaxy evolution since cosmic dawn.

[1] The value calculated by A. I. Hartley et al. (2023) is given in physical units, however, all observations are given in comoving units. Therefore, the number density obtained by A. I. Hartley et al. (2023) in comoving units (with $5/(302.6\ \mathrm{cMpc})^3 \approx 1.8 \times 10^{-7}\ \mathrm{cMpc}^{-3}$) is about 2 orders of magnitude smaller than the observations.

2. Simulations and Observations

Finding quenched galaxies at high redshifts requires a box volume large enough to encompass all potential environments while at the same time the simulation needs to have high enough resolution to properly resolve galaxies with stellar masses larger than $1 \times 10^{10}\ M_\odot$ to capture the observed mass ranges of quiescent galaxies. We use Box3 with a volume of $(128\ \mathrm{Mpc}\ h^{-1})^3$ from the fully hydrodynamical cosmological simulation suite Magneticum Pathfinder[2] in ultrahigh resolution (UHR), with dark matter, gas, and stellar particles masses of $m_{\mathrm{dm}} = 3.6 \times 10^7\ M_\odot\ h^{-1}$, $m_{\mathrm{gas}} = 7.3 \times 10^6\ M_\odot\ h^{-1}$, and $m_* \approx 0.25 m_{\mathrm{gas}} \approx 1.8 \times 10^6\ M_\odot\ h^{-1}$, respectively, as every gas particle spawns up to four stellar particles. Gravitational softening for the three components is included as $\epsilon_{\mathrm{dm}} = \epsilon_{\mathrm{gas}} = 1.4\ \mathrm{kpc}\ h^{-1}$ and $\epsilon_* = 0.7\ \mathrm{kpc}\ h^{-1}$. The simulation uses a Wilkinson Microwave Anisotropy Probe 7 cosmology following E. Komatsu et al. (2011), with $h = 0.704$, $\Omega_{\mathrm{m}} = 0.272$, $\Omega_{\mathrm{b}} = 0.0451$, $\Omega_\Lambda = 0.728$, $\sigma_8 = 0.809$, and an initial slope of the power spectrum of $n_{\mathrm{s}} = 0.963$.

The simulation was performed with an updated version of GADGET-2 (V. Springel 2005), with modifications to smoothed particle hydrodynamics, including artificial viscosity and thermal conductivity, according to K. Dolag et al. (2004, 20050, J. Donnert et al. (2013), and A. M. Beck et al. (2016). It includes full baryonic physics as described in detail by A. F. Teklu et al. (2015). Star formation and stellar feedback are implemented based on the model by V. Springel & L. Hernquist (2003). Stellar feedback encompasses feedback from Type I and Type II supernovae and asymptotic giant branch stars, with metal enrichment and cooling from all three sources are implemented according to L. Tornatore et al. (2004, 2007) and R. P. C. Wiersma et al. (2009). The assumed initial mass function is given by G. Chabrier (2003). In addition, UV/X-ray background and cosmic microwave background radiation are computed according to F. Haardt & P. Madau (2001).

Black hole treatment and feedback is included as described by L. K. Steinborn et al. (2015) based on the model by D. Fabjan et al. (2010) and M. Hirschmann et al. (2014). Typically, AGN are seeded in lower-mass galaxies and then grow through accretion or mergers with other black holes. This mass growth is dependent on the surrounding gas density and velocity relative to the black hole, with higher density and lower velocity resulting in higher accretion following the Bondi prescription of $\dot{M}_{\mathrm{B}} \propto \alpha\rho/(c_{\mathrm{s}}^2 + v^2)^{3/2}$. Limited resolution reduces the efficiency of the mass accretion, such that a boost factor α is usually applied. The implemented changes by L. K. Steinborn et al. (2015) concern both the accretion and feedback. For the former, instead of determining the density ρ and relative velocity v of the total gas present, the model differentiates cold and hot gas into two separate accretion rates with their own boost factors.

The boost factor for the hot phase is 10, as hot gas generally more closely follows the assumptions used for the Bondi model of a hot isothermal medium. For cold gas, the boost factor is 100 due to their more efficient feeding as shown by high-resolution simulations (M. Gaspari et al. 2013). This means that even when the galaxy is generally dominated by a hot phase, cold streams can still efficiently grow the black hole, resulting in a faster growth at higher redshifts while reducing the

[2] http://www.magneticum.org

accretion at intermediate redshifts. L. K. Steinborn et al. (2015) show that this more accurately reproduces observed scaling relations.

Finally, the feedback itself is changed by L. K. Steinborn et al. (2015), with a smoother transition between quasar and radio mode efficiencies as well as making the radiative feedback efficiency increase with black hole mass following observational findings. This results in lower feedback of highly accreting low-mass black holes.

Galaxies are identified using SUBFIND (V. Springel et al. 2001; K. Dolag et al. 2009). In a nutshell, SUBFIND identifies structure linked by a friends-of-friends algorithm. It then detects saddle points in the potential of these linked "halos," which are then used to identify separate "subhalos," which represent individual galaxies. Galaxies that SUBFIND identifies as the most massive galaxy in a given halo are called "central" galaxies, while we call all galaxies that are not the centrals of their host halo "satellite" galaxies. Galaxies are traced forward and backwards in time using L-BaseTree (V. Springel et al. 2005). Toward higher redshifts, the most massive galaxy at each snapshot is used as the main progenitor, and that branch of the merger tree is followed. Tracing forward, we mark those galaxies that merge with a larger galaxy, i.e., that are the smaller partner in the merger event, as "central subs," since the remnant galaxy after the merger is still a central, but the galaxy we were tracing was the minor contributor to the mass growth and thus not the main branch itself. This procedure works until the last high-resolution snapshot at $z \approx 2$.

The simulation Box3 UHR simulation ran until $z \approx 2$, covering the redshift evolution with outputs since $z \approx 15$. Most importantly, it provides a snapshot with full particle information at $z = 3.4$, which is comparable to the average redshift at which the quenched galaxies presented by T. Nanayakkara et al. (2022) and A. S. Long et al. (2024) are observed. At $z = 3.4$, 2903 galaxies are found with stellar masses above $M_* > 2 \times 10^{10}\ M_\odot$, above which we consider galaxies to be resolved well enough to be included in this study for more than pure number counting aspects.

To trace halos at redshifts below $z \approx 2$, we match halos at the last available snapshot to the halos in the simulation Box3 high-resolution simulation, which ran until $z = 0$ with the same initial conditions (ICs) but a lower resolution, and track those forward to $z = 0$. The high-resolution simulations have dark matter, gas, and stellar particles masses of $m_{\rm dm} = 6.9 \times 10^8\ M_\odot\ h^{-1}$, $m_{\rm gas} = 1.4 \times 10^8\ M_\odot\ h^{-1}$, and $m_* \approx 0.25 m_{\rm gas} \approx 3.5 \times 10^7\ M_\odot\ h^{-1}$, respectively, and gravitational softening of $\epsilon_{\rm dm} = \epsilon_{\rm gas} = 3.75$ kpc h^{-1} and $\epsilon_* = 2$ kpc h^{-1}. Note that all simulations in Magneticum with the same box size have the same ICs, and the lower-resolution ICs were generated through downsizing of the higher-resolution ICs.

Matching was done by taking all galaxies in the high-resolution box within 500 ckpc (≈100 physical kpc) around the original galaxy location in the UHR box. Of these, we match to the galaxy with the most similar total subhalo mass $M_{\rm tot}$ (baryonic plus dark matter). Note that we also compared what happens when matching to the halo with the most similar total halo mass $M_{\rm 200crit}$ (instead of using the galaxies themselves), which produced identical matches for 98% of the galaxies. Generally, we find that for 92% of matched galaxies the comoving separation is less than 200 ckpc and the total halo mass $M_{\rm 200crit}$ is within 0.1 dex (≈25%).

Due to the lower resolution of the high-resolution simulations compared to the UHR simulation, we only use global information like total galaxy (or halo) mass to track down to $z = 0$. While overall at redshifts below $z < 5$, global properties like star formation rate densities, halo mass functions, and stellar mass functions converge between the simulation runs within the mass ranges that the resolution allows (see M. Hirschmann et al. 2014; L. C. Kimmig et al. 2023), on an individual galaxy basis this might differ strongly. This may be due to differences in feedback or the timing of star formation events, as well as the larger smoothing in the high-resolution simulations, which all impact parameters such as star formation rate, stellar size, or stellar mass. Therefore, we do not attempt to compare these properties between the two simulation runs, but only use the halo properties to track down the evolution of the total halo mass and the environment at the end of this work.

3. Quenched Galaxies at $z \approx 3.4$

Observed quiescent galaxies with full spectra have recently been reported by T. Nanayakkara et al. (2022) and A. C. Carnall et al. (2023) using JWST NIRISS spectra at redshifts of $z \approx 3$–4, enabling examination of the stellar age distributions and thus the quenching and formation times of these galaxies. In the following, we identify quenched quiescent galaxies at a redshift of $z = 3.4$ in the simulations and compare their global properties to their observed counterparts.

Throughout this work we consider galaxies with three different stellar mass cuts: (I) a stellar mass of $M_* \geqslant 2 \times 10^{10}\ M_\odot$, for which star formation properties are well enough resolved to safely identify quiescent galaxies; (II) a stellar mass of $M_* \geqslant 3 \times 10^{10}\ M_\odot$, where these are well resolved with more than 10,000 stellar particles; and (III) a stellar mass of $M_* \geqslant 5 \times 10^{10}\ M_\odot$, encompassing the best resolved and most massive galaxies at the given redshift. At $z = 3.42$, this encompasses 2903 galaxies in cut (I), and 1309 galaxies above the most important cut level (II), of which 1217 are centrals and 92 are satellite galaxies. Above the third cut range, cut (III), we find 395 galaxies.

We define galaxies as "fully quenched" if their current star formation rate is in fact zero, which means given the resolution of our simulation that it is below $10^{-3}\ M_\odot\ {\rm yr}^{-1}$. At $z = 3.4$, for our three mass cuts this leads to 109 quenched galaxies in cut (I) of stellar mass larger than $M_* \geqslant 2 \times 10^{10}\ M_\odot$, and 36 quenched galaxies of cut (II) with $M_* \geqslant 3 \times 10^{10}\ M_\odot$, being 28 centrals and eight satellites. In our highest mass cut (III), we find six quenched galaxies with $M_* \geqslant 5 \times 10^{10}\ M_\odot$, two of which are satellites and four are centrals. This is the sample we study here in detail, see also the according discussion on that by K25.

However, observationally measuring zero star formation is not actually zero but limited by what can still be detected. Therefore, "quenched" is usually defined using the specific star formation rate (sSFR), i.e., galaxies with ${\rm sSFR} < 0.3 \times t_{\rm Hub}$ are defined as quiescent (M. Franx et al. 2008).[3] Alternatively, at high redshifts a slightly adapted version of this is used as introduced by A. C. Carnall et al. (2020), where quiescence is defined as ${\rm sSFR} < 0.2 \times t_{\rm Hub}$. At $z = 3.4$, for our three mass cuts this leads to 722 (620) quenched galaxies in cut (I) of stellar mass larger than $M_* \geqslant 2 \times 10^{10}\ M_\odot$, and 352 (301)

[3] This is also the method that was used by R.-S. Remus et al. (2023) to predict quiescent fractions for different halo masses through cosmic time up to $z = 4.2$.

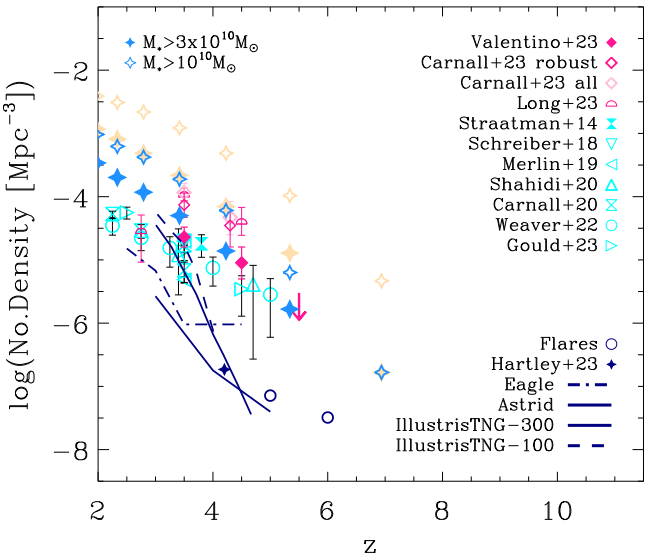

Figure 1. Number densities of quenched (blue) and nonquenched (sand) galaxies with stellar masses above 3×10^{10} $M_{\odot}$ (filled) and 1×10^{10} $M_{\odot}$ (open), as a function of redshift. Pink symbols show the observed number densities of quenched galaxies with $M_{*} > 3 \times 10^{10}$ $M_{\odot}$ obtained with JWST from F. Valentino et al. (2023, filled diamonds and downward pink arrow), A. S. Long et al. (2024, open half circles), and A. C. Carnall et al. (2023, open diamonds, dark pink for their robust sample, light pink for all). Cyan data points present pre-JWST measurements of quenched number densities from C. M. S. Straatman et al. (2014, filled hourglass), C. Schreiber et al. (2018, downward triangles), E. Merlin et al. (2019, leftward triangles), A. Shahidi et al. (2020, upward triangles), A. C. Carnall et al. (2020, open hourglass), J. R. Weaver et al. (2023, open circles), and K. M. L. Gould et al. (2023, rightward triangles). The number densities reported for different simulations in comparable mass cuts are shown in dark blue, i.e., IllustrisTNG-300 (solid line), IllustrisTNG-100 (dashed line), and Astrid (dashed–dotted–dot–dotted line) from E. J. Weller et al. (2025), Eagle (dashed–dotted line) from A. S. Long et al. (2024), IllustrisTNG-300 (filled diamond) from A. I. Hartley et al. (2023), and Flares (open circles) from K. M. L. Gould et al. (2023).

quenched galaxies of cut (II) with $M_{*} \geqslant 3 \times 10^{10}$ $M_{\odot}$, being 315 (270) centrals and 37 (31) satellites. In our highest mass cut (III), we find 97 (81) quenched galaxies with $M_{*} \geqslant 5 \times 10^{10}$ $M_{\odot}$, of which 11 (9) are satellites and 86 (72) are centrals, using the criterion by M. Franx et al. (2008) or A. C. Carnall et al. (2020), respectively.

Before we study the details of our fully quenched galaxy sample, we first test if the number densities of quenched galaxies in the simulation is in agreement with observations. Here, we use the criterion of M. Franx et al. (2008) as this is most commonly used in the literature to which we compare here, but we note that the differences between the results using the M. Franx et al. (2008) or the A. C. Carnall et al. (2020) criteria are so small they the data points for the number densities actually overlap, which is why we chose to show the results from the more commonly used M. Franx et al. (2008) criterion. Figure 1 shows the number densities of quenched (blue) and nonquenched (sand) galaxies from $z = 2$ to $z = 10$, for two different stellar mass cuts (open symbols: $M_{*} > 1 \times 10^{10}$ $M_{\odot}$, filled symbols: 3×10^{10} $M_{\odot}$). Generally, the number density of both quenched and all galaxies increases similarly with redshift. Quenched galaxies appear later than nonquenched galaxies of similar mass, with the first quenched galaxies with stellar masses above $M_{*} > 1 \times 10^{10}$ $M_{\odot}$ appearing around $z = 5.5$. This does not imply that there are no quenched galaxies at higher redshift, but rather that the simulated volume with a 128 Mpc h^{-1} box length is still too small to have massive galaxies appear at redshifts as high as $z = 8$, as discussed in more detail in the companion paper (K25). In addition, there are a few massive galaxies in our simulation that are quenched at higher redshifts, but rejuvenate until the point of measurement at $z = 3.4$. One of these galaxies is shown in K25 in more detail, and we will come back to this point later in this study.

Furthermore, Figure 1 also provides a comparison to current observed quenched number densities from JWST (filled pink diamonds: F. Valentino et al. 2023; open pink diamonds: A. C. Carnall et al. 2023; pink half circles: A. S. Long et al. 2024) using NIRCam imaging and a lower mass cut of about 3×10^{10} $M_{\odot}$ comparable to the filled blue symbols from the simulation. We find overall very good agreement, in particular we see the same increase in the number density when going from a redshift of around $z = 5$ to $z = 3.4$. We do not find as decrease to $z = 2.8$ as reported by A. S. Long et al. (2024), however, this could also be due to noncompleteness in that measurement. JWST measurements of quenched number densities at lower redshifts are still missing, but generally, it can be seen that the number densities of quenched galaxies increase in the JWST measurements compared to the pre-JWST measurements of quenched number densities that are included in the figure as cyan symbols. Note that we only included the spectroscopic JWST measurements, as photometric measurement contamination from dusty galaxies at $z \approx 2$ is still a matter of concern (B. Forrest et al. 2024). Compared to the pre-JWST, our simulation tends to produce slightly larger number densities of quenched galaxies at redshifts below $z = 3$, however, going down from $z = 4$ to $z = 0$, L. K. Steinborn et al. (2015) have show in a previous study using the same physics as the simulation used in this work that the number densities end up matching those from observations quite well again at the lowest redshifts.

While it remains to be seen whether follow-up JWST observations also find enhanced quenched number densities at lower redshifts or if the AGN feedback should be further refined, or both, it is clear that our simulation manages to capture the JWST observations at high redshift, in particular above $z = 4$, where it has been reported previously that simulations struggle to reproduce these high number densities (A. S. Long et al. 2024). To demonstrate this issue, the number densities of quenched galaxies of different known simulations from the literature are also included in Figure 1 as dark blue lines and symbols, if comparable stellar mass cuts were available. More explicitly, values are included for Astrid, IllustrisTNG-300, and IllustrisTNG-100 from E. J. Weller et al. (2025); Eagle (A. S. Long et al. 2024); and Flares (K. M. L. Gould et al. 2023). In addition, we included the quenched galaxy number density reported for the IllustrisTNG-300 simulation by A. I. Hartley et al. (2023) at $z \approx 4.2$ as a dark blue diamond.[4]

The differences between the simulations originate from the different subgrid physics implementations, most likely the AGN feedback. For example, for IllustrisTNG both A. I. Hartley et al. (2023) and S. Kurinchi-Vendhan et al. (2024) show that quenching is due to the implemented AGN feedback as soon as the kinetic feedback kicks in. This kinetic feedback and

[4] Note that we adapted the data point from the paper to comoving units, as the value presented by A. I. Hartley et al. (2023) was given in physical units (see also E. J. Weller et al. 2025, for this point), while all the observations are given in comoving units.

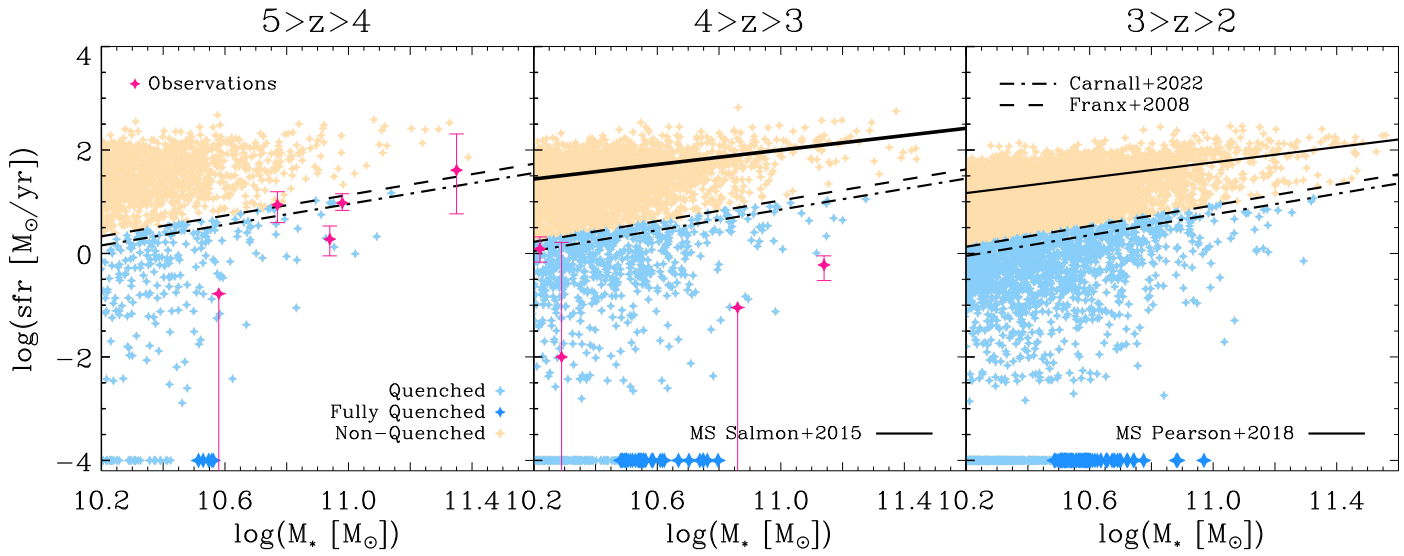

Figure 2. The star formation rate of Magneticum galaxies at different redshift ranges as a function of stellar mass. From left to right: $5 > z > 4$, $4 > z > 3$, and $3 > z > 2$. Galaxies with a star formation rate $= 0$ are placed at $\log(\mathrm{sfr}[M_\odot\ \mathrm{yr}^{-1}]) = -4$ and defined as "fully quenched" (dark blue). Galaxies with star formation rates below the Franx criterion of $\mathrm{sSFR} < 0.3 \times t_{\mathrm{Hub}}$ are defined as "quenched" (light blue). All other galaxies have ongoing star formation and are defined as "nonquenched" (sand). The black solid line represents the observed star-forming main sequence at $z = 4$ from B. Salmon et al. (2015) and at $z \approx 2$ from W. J. Pearson et al. (2018). The black dashed lines mark the criterion by M. Franx et al. (2008), while the black dashed–dotted lines mark the adapted criterion from A. C. Carnall et al. (2020). Observations of quenched galaxies from the literature are included as magenta diamonds, compiled from J. Antwi-Danso et al. (2025), A. de Graaff et al. (2025), S. M. Urbano Stawinski et al. (2024), and T. Kakimoto et al. (2024).

its efficiency are coupled to the black hole mass, which itself correlates with the stellar mass of the galaxies, and thus quenching is inevitable by construction for galaxies above a given stellar mass in these simulations. In Magneticum, the main driver of the difference is that the prescription differentiates accretion onto the black hole in terms of cold or hot gas, as described in more detail in Section 2 and by L. K. Steinborn et al. (2015). By using different boost factors for these two accretion modes, Magneticum allows for more diverse black hole mass histories. A stream of cold gas can still be accreted efficiently (and thus result in a large black hole growth and subsequent feedback event) even if the surrounding gas is hot, as we do not smooth over both modes. Simultaneously, if the cold gas forms a disk, the high relative velocity will naturally reduce the amount of accretion, even if the surrounding hot gas has a lower relative velocity (again, because we do not smooth over the two modes).

Overall, the similarity in quenched number densities from observations and the Magneticum simulations is promising, so we will now study the properties of the simulated quenched galaxies at a representative redshift of $z = 3.4$, the snapshot closest to the redshifts of the observed samples of quiescent galaxies from JWST (T. Nanayakkara et al. 2022; A. C. Carnall et al. 2023; A. S. Long et al. 2024) in more detail.

3.1. Global Properties

First, we test the general properties of the quenched galaxies compared to the nonquenched galaxies from our simulations and compare with the available observations from the literature. Figure 2 shows the star formation rate of the galaxies against stellar mass, the so-called star formation main sequence, at three different redshift ranges of $5 > z > 4$, $4 > z > 3$, and $3 > z > 2$ for all galaxies in the simulation (sand color). We find that most of the galaxies lie around the star-forming main sequence, as observed by B. Salmon et al. (2015) at $z \approx 4$ from the CANDELS survey and by W. J. Pearson et al. (2018) at $z \approx 2$.

As expected, there are, however, some galaxies which scatter down toward lower star formation rates, and the commonly used cuts for what is called quiescence by M. Franx et al. (2008) and A. C. Carnall et al. (2020) are shown as dashed and dashed–dotted lines, respectively. All galaxies with star formation rates below the M. Franx et al. (2008) criterion are shown in light blue. Those galaxies with no ongoing star formation at all, which are therefore classified as fully quenched, are shown in blue (with their logarithmic star formation rate artificially set to -4 so that they can be included in the figure despite their real star formation rate being zero). The galaxies that are targeted in this work are those shown in blue in the middle panel. This visualizes our selection criterion while also showing that the simulations successfully reproduce the star formation main sequence and thus can be utilized for this study. For comparison, we also included several data sets compiled from observations by J. Antwi-Danso et al. (2025), A. C. Carnall et al. (2024), A. de Graaff et al. (2025), S. M. Urbano Stawinski et al. (2024), and T. Kakimoto et al. (2024) as pink diamonds. As can clearly be seen, our simulation captures all of the observed quenched galaxies in its range.

Interestingly, none of the quenched galaxies from the simulations is among the most massive galaxies at $z = 3.4$. Even more so, most of the massive galaxies are actually on the main sequence, heavily forming stars. This already indicated that the quenched galaxies are, in fact, not hosted by the most massive nodes in the cosmic web at that redshift, but we will return to this in more detail soon. Note that we here already see a difference to the results reported for the IllustrisTNG simulations by A. I. Hartley et al. (2023) and S. Kurinchi-Vendhan et al. (2024), as in these simulations the quenched galaxies are the most massive ones in the sample.

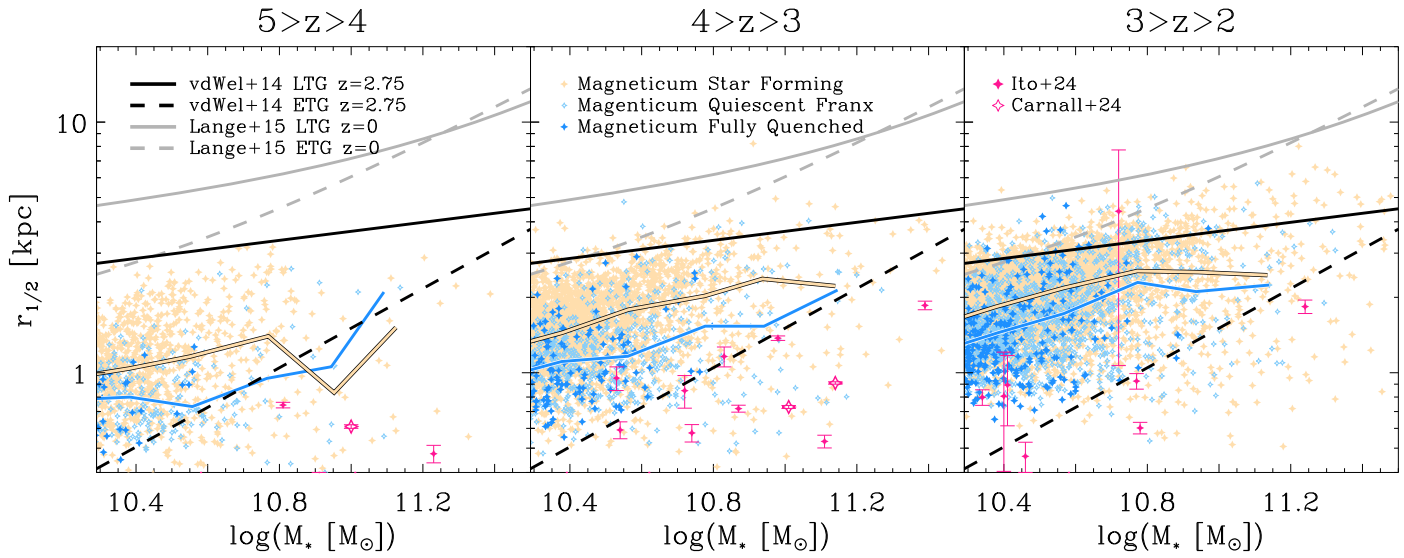

Figure 3. Stellar mass–size relation of all Magneticum galaxies (sand diamonds), with the quenched galaxies according to M. Franx et al. (2008) shown in light blue and the fully quenched galaxies shown in blue. Sand and blue solid lines mark the median values for the nonquenched and quenched galaxies, respectively. Black lines mark the relations found for early-type (dashed) and late-type (solid) galaxies at $z = 2.75$ from A. van der Wel et al. (2014), while gray lines mark early-type (dashed) and late-type (solid) relations at $z = 0$ from R. Lange et al. (2015) from the GAMA survey for comparison. From left to right: $5 > z > 4$, $4 > z > 3$, and $3 > z > 2$. Observations from A. C. Carnall et al. (2024) and K. Ito et al. (2024) are included as open and filled pink diamonds, respectively.

Before we look at the host halo masses of the quenched galaxies, we study the mass–size relation of the simulated galaxies at the same three different redshift ranges of $5 > z > 4$, $4 > z > 3$, and $3 > z > 2$ $z = 3.4$ as in Figure 2 and Figure 3. The simulated galaxies (sand diamonds) clearly lie within the observed range of sizes for a given mass that are found at high redshifts, indicated by the black lines for galaxies at $z = 2.75$ from A. van der Wel et al. (2014), and not within the size range observed at $z = 0$ marked in gray (GAMA survey; R. Lange et al. 2015). As shown already by F. Schulze et al. (2018), the Magneticum simulation in the UHR simulation successfully reproduce the mass–size relation of galaxies at $z = 0$, and they also reproduce the change in mass–size relation with redshift from $z = 2$ to $z = 0$ for early-type galaxies (R.-S. Remus et al. 2017). From Figure 3 we clearly see from the left to the right panel that this trend of generally having smaller galaxy sizes for a given stellar mass at higher redshifts continues to even higher redshifts than $z = 2$, in good agreement with the observed trends by A. van der Wel et al. (2014) and also with size evolution trends reported from JWST up to $z \approx 5$ from K. Ito et al. (2024) and A. C. Carnall et al. (2024).

Figure 3 also reveals that the quenched galaxies (blue diamonds) in our sample on average have smaller sizes at a given stellar mass than the overall sample (sand diamonds), albeit the scatter is similarly large. We do not find a correlation between the stellar mass of the quenched galaxies and their formation redshift, but there is a slight tendency for quenched galaxies that have formed earlier to be larger in size than those that have formed more recently at a fixed stellar mass. We also included in the figure as pink data points the observed quenched galaxies from K. Ito et al. (2024) and A. C. Carnall et al. (2024). While the overall behavior is, as mentioned above, in qualitative agreement, we also note that the actual sizes of the observed quiescent galaxies are generally smaller than those reported from the simulation. This is due to the limitations of our softening, which prevents sizes to be smaller than its value by smearing out the distribution of the matter in this region. Thus, capturing the size evolution despite the limitations of the resolution is promising, but also highlights the need for even better resolved simulations in the future to study the radial properties of galaxies.

3.2. Environment

Coming back to the question of the environment of the quenched galaxies, Figure 4 depicts the projected surface brightness of the gas in Box3 (UHR) at $z = 3.4$, which is a measure for the temperature of the gas as brighter surface brightness corresponds to a higher temperature of the gas. The positions of the six most massive quenched galaxies are marked by black circles. They appear to inhabit diverse regions of the cosmic web, though none of them lie at the centers of the hottest, most dense regions. Instead, they lie adjacent (leftmost and central two), removed (two rightmost), or even entirely isolated (top most) from the more pronounced filaments of the cosmic web. We tested this for all 28 quenched galaxies above a stellar mass of $M_* \geqslant 3 \times 10^{10}\ M_\odot$, and found all of them to live in rather remote or adjacent regions of the developing cosmic web, never in the main nodes. This suggests that quenching at high redshifts is not efficient in the densest environments albeit the AGN feedback is strongest for the most massive galaxies, indicating that the processes that lead to quenching of galaxies at high redshifts are more complicated than the simple picture of AGN feedback quenching the galaxy.

Despite not being the most massive structures in the simulation, all of the quenched halos exhibit a bubble of heated gas surrounding them, reaching out to several virial radii. Note that this is difficult to see for some of these halos in Figure 4 as the figure shows the whole box volume and therefore the individual halos are actually small. The fact that the bubbles can be clearly seen for some of the marked halos (for example the uppermost quenched halo) demonstrates how large these bubbles can become. The origin of these bubbles is discussed in the companion paper (K25) to be the result of their rapid quenching process, driven outward by the feedback from the AGN.

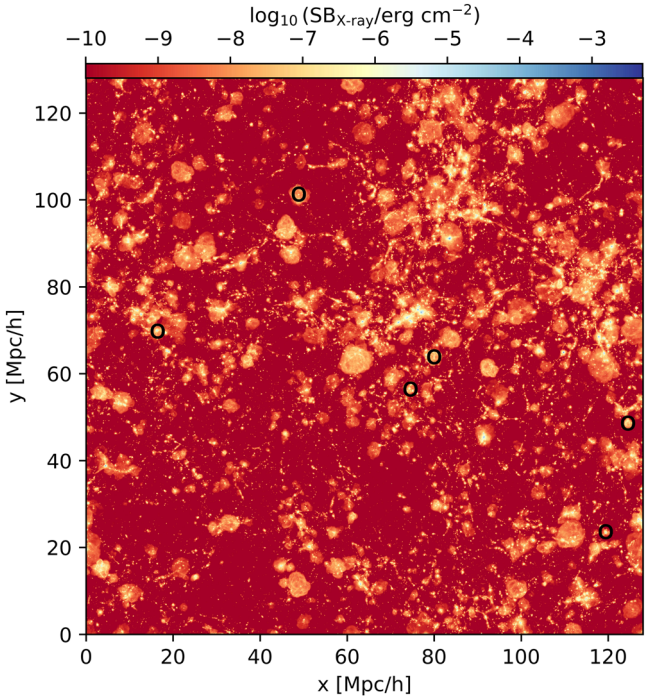

Figure 4. Projected surface brightness of the gas of the full Box3 UHR simulation at $z = 3.4$. Black circles mark the six most massive quenched galaxies. This is actually a measure for the temperature of the gas, as the surface brightness is brighter the hotter the gas.

This is in agreement with what we had seen before already, namely that the quenched galaxies are not among the most massive galaxies. The left panel of Figure 5 further strengthens this point: Shown is a histogram of the virial masses of the quenched (dark blue, dotted) and all (sand, solid) galaxies with stellar masses above $M_* > 2 \times 10^{10}\ M_\odot$, albeit the latter is scaled to match the numbers of the quenched galaxies for better comparison of the distributions. On first glance, both distributions appear to be similar, with a tendency for the quenched galaxies to be overly common at small virial masses around $M_{\rm vir} \approx 5 \times 10^{11}\ M_\odot$, which is around the Milky Way mass range.

However, this picture changes once we split the quenched sample into central galaxies (solid blue line) and satellite galaxies (dashed light blue line). The quenched sample clearly divides in halo mass, with all quenched galaxies in halos of virial masses above $M_{\rm vir} \approx 2 \times 10^{12}\ M_\odot$ being satellites, i.e., they were accreted onto a more massive dark matter halo, and they are not the central galaxies of the massive nodes. Those quenched galaxies that are central galaxies all live in smaller mass halos, clearly supporting the idea that the environment of a galaxy is crucial for quenching to happen at high redshifts.

3.3. Formation Redshifts—When do the Quenched Galaxies Form?

Given that the quenched galaxies are already rather massive at $z = 3.4$, the question arises when they had actually formed their stars, and whether or not they already differ from nonquenched massive galaxies with respect to their formation times. To this end we define $z_{\rm form}$ here as the redshift at which half of the galaxy's total stellar mass at $z = 3.4$ has been formed. The right panel of Figure 5, shows a histogram of the formation redshifts of all galaxies (sand) and the quenched galaxies (blue). As can be seen most galaxies have formed their stars around a redshift of $z_{\rm form} \approx 4$, though there is some scatter toward formation redshifts as high as $z_{\rm form} \approx 7$. The quenched galaxies, both centrals and satellites, have on average formed earlier than the nonquenched galaxies, with the satellites having even earlier formation redshifts than the centrals. These high formation redshifts found for the quenched galaxies are in broad agreement with those found in observed quenched galaxies by T. Nanayakkara et al. (2022, magenta triangles) and A. C. Carnall et al. (2023, magenta line). It should be noted, however, that the only quenched galaxy which matches the earliest two times of $z_{\rm form} \approx 7$ found by T. Nanayakkara et al. (2022) ends up being a satellite galaxy at $z = 3.4$.

Nevertheless, we do not have a quenched galaxy with a formation redshift larger than $z = 7$, and thus no counterpart for the quenched galaxy reported by K. Glazebrook et al. (2023) to exhibit a formation redshift around $z = 11$. However, earlier formation redshifts can be found in our sample of galaxies if we identify quenched galaxies at $z \approx 5$. Observed at that redshift, we even have a quenched galaxy with a formation redshift before $z = 8$, as shown by K25. Interestingly, that galaxy rekindles its star formation at about $z \approx 4$, and is no longer quiescent at $z = 3.4$.

All observed quenched galaxies at around $z = 3.4$ are rather massive in stellar mass, so the question arises if the formation redshift is connected to the stellar mass. Figure 6 shows the stellar mass against the formation redshift for the quenched (blue) and nonquenched galaxies (sand) for the simulations, including the observed quenched galaxies (magenta). There is no apparent correlation between the stellar mass either of the quenched or nonquenched galaxies, neither in the simulations nor the observations.

However, while the simulation includes quenched galaxies with masses and formation redshifts comparable to the observations by T. Nanayakkara et al. (2022) and A. C. Carnall et al. (2023) at the mass range from $3 \times 10^{10}\ M_\odot$ to $6 \times 10^{10}\ M_\odot$, we also clearly see that we do not recover the extremely massive quenched galaxies that are part of the observed sample. The most extreme stellar masses around $10^{11}\ M_\odot$ are found only for galaxies which are actively forming stars. There are, however, six quenched galaxies with masses which are in excess of $5 \times 10^{10}\ M_\odot$: ID4180, ID5058 (for the two satellites) and ID16396, ID18258, ID20633, and ID22007 (for the four centrals).

Figure 7 shows the fraction of stars which are formed at a given redshift for these six most massive quenched galaxies (solid lines) as well as their formation redshifts $z_{\rm form}$ (vertical dashed–dotted lines). They exhibit diverse stellar formation histories, with galaxy ID5058 (purple) in particular having formed most of its stars very early on. This galaxy is also quenched at an earlier time, with only around 5% of its stars formed after $z = 5$ and practically none after $z = 4$. Although it is a satellite at $z = 3.4$, it was still a central at $z = 4.2$ and thus the quenching did not occur due to the environment of the host. In fact, it is quenched in a similar process like the other central galaxies and afterwards accreted by the more massive structure, which also prevents any kind of rejuvenation.

By contrast, galaxies ID18258 and ID22007 (salmon and yellow) exhibit a strong starburst right around $z = 4$, resulting in a much more recent $z_{\rm form}$. The former in particular has an interesting stellar buildup, with three distinct peaks of star

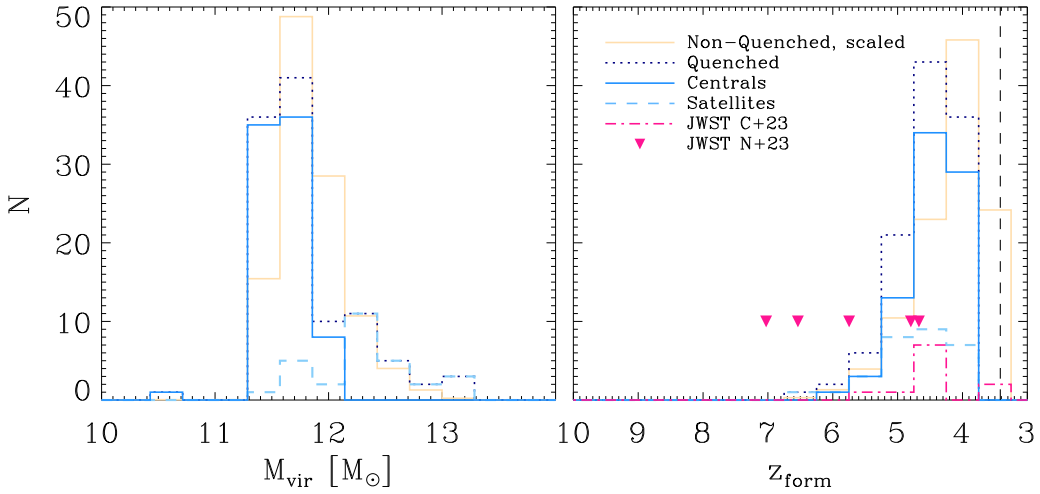

Figure 5. Left: histogram of the virial masses of the host haloes of the quenched galaxies (blue dotted) and nonquenched galaxies (sand solid line, scaled down to match) with stellar masses above $2 \times 10^{10}\ M_\odot$. The solid blue and dashed blue lines denote quenched galaxies which are centrals and satellites, respectively. Right: histogram of the formation redshifts z_{form}, colored as in the left panel. In addition, observations from JWST are included in pink: the dashed–dotted line marks the formation redshift distribution of JWST CEERS quenched galaxies observed between $z = 4$ and $z = 3$ from A. C. Carnall et al. (2023). The solid triangles mark the formation redshifts of the five galaxies from T. Nanayakkara et al. (2022) with spectroscopic NIRSpec data.

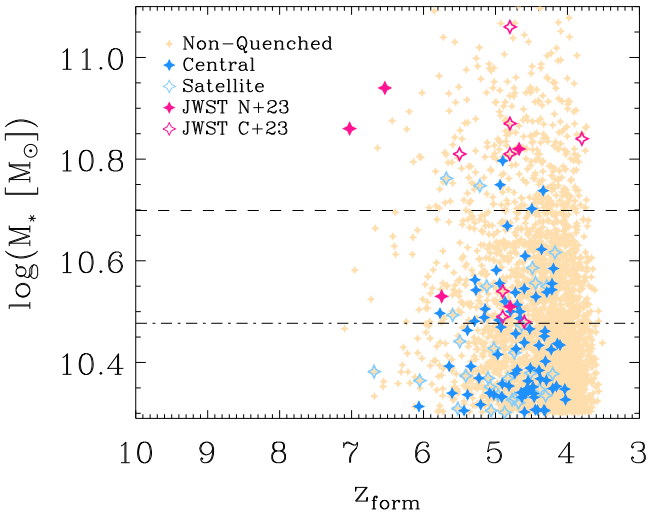

Figure 6. Stellar mass as a function of the formation redshift for the star-forming (sand) and quenched galaxies (blue stars), with the latter further differentiated between centrals (filled) and satellites (open) defined at redshift $z = 3.4$. Also plotted are observed quenched galaxies from T. Nanayakkara et al. (2022) and A. C. Carnall et al. (2023, filled and open pink symbols, respectively). The black horizontal lines indicate stellar masses of 5 (dashed) and $3 \times 10^{10}\ M_\odot$ (dashed–dotted).

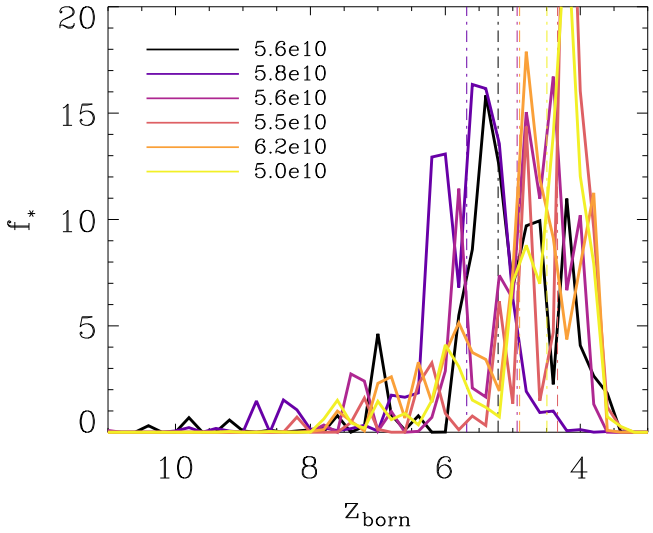

Figure 7. The fraction of stars as a percentage formed at a given redshift for each of the six most massive quenched galaxies. Vertical colored dashed–dotted lines denote their z_{form}, while the label denotes their stellar mass at $z = 3.4$ (sorted in order of their IDs).

formation in sequence at $z \approx 5.2$, 4.8, and then the final at $z = 4$.

All six galaxies show generally bursty star formation, with significant fractions (>10%) of their final stellar mass formed in these short peaks, usually then followed by dips. As these are the binned formation redshifts of individual stellar particles, this burstiness is not a result of a lack of temporal resolution of snapshot outputs but rather physical in origin. Strong star formation results in higher stellar feedback, which in turn can then briefly inhibit the formation of new stars thus causing a dip.

It is interesting to note that although this interplay of star formation and feedback had been active in all six galaxies from around $z = 6$, they retain significant star formation also during the dips and it is not until close to $z = 3.4$ that they fully quench. The final mechanism required to result in a full stop of their star formation is the feedback from the central supermassive black hole, in combination with their environment, which is discussed in more detail in the companion paper (K25).

The time of quenching, z_{quench}, is defined as the redshift at which the last star in the galaxy as seen at $z = 3.4$ has formed. The top panel in Figure 8 shows z_{quench} as a function of M_* for all quenched galaxies with $M_* > 3 \times 10^{10}\ M_\odot$ (light blue symbols), and the fully quenched galaxies (blue). We find z_{quench} between $z = 3$ and $z = 6.5$, similar to the observed values of T. Nanayakkara et al. (2022) aside from their most striking outlier. Most of the galaxies from A. C. Carnall et al. (2024) and the galaxy from A. de Graaff et al. (2025) have earlier quenching times, but are also generally more massive than the bulk of our sample of quenched galaxies, which is most likely a result of our simulated box volume still being too

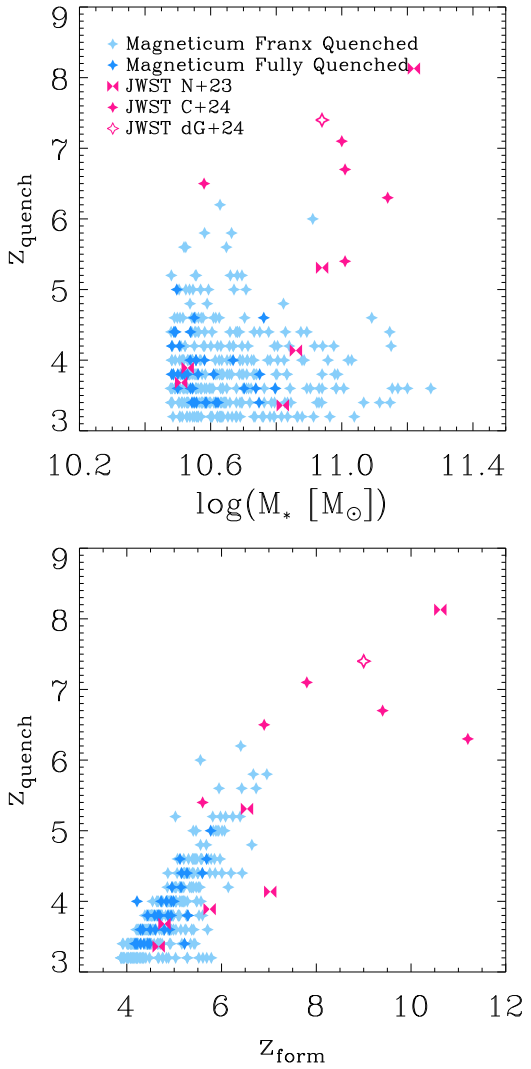

Figure 8. $z_{\rm quench}$ vs. M_* (top) and $z_{\rm form}$ (bottom) for all simulated quenched galaxies (light blue), the fully quenched sample (blue), and the values of observed galaxies from T. Nanayakkara et al. (2022, pink bow ties), A. de Graaff et al. (2025, pink open diamond), and A. C. Carnall et al. (2024, pink filled diamonds).

small to reproduce the most massive galaxies at these redshifts in a statistically representative matter as discussed by K25. There is no clear additional trend with stellar mass visible, neither in the simulation nor the observations, indicating that the process that quenches galaxies at high redshifts in fact is not directly correlated to the galaxy mass but rather other effects come to play. As discussed by K25, these are a combination of the feedback from the stars, the AGN feedback, and the environment being underdense; this is different than what has been found by A. I. Hartley et al. (2023) and S. Kurinchi-Vendhan et al. (2024) for IllustrisTNG, where the quenching is correlated with the mass of the galaxies due to the implemented feedback.

Interestingly, the formation redshift $z_{\rm form}$ and the quenching redshift $z_{\rm quench}$ are correlated, as shown in the lower panel of Figure 8. Galaxies with younger formation redshifts also have lower quenching redshifts, meaning that more recent quenching also implies that half the total stellar mass was formed more recently. This is in agreement with the result that the quenching of the galaxies is preceded by a spike in star formation that forms most of the stars in the galaxy. And while the simulation does not recover the high formation and quenching redshifts of the most extreme outlier from the observations by T. Nanayakkara et al. (2022; which is also the galaxy discussed in more detail by K. Glazebrook et al. 2023), we clearly see that it lies around where one would expect from the simulated sample when extending the correlation to higher formation redshifts.

This clearly indicates that the quenched galaxies form most of their stars both in simulations and observations rather quickly in a short time period prior to the very quick quenching event, in agreement with what is discussed by K25. It also shows that this process of quenching must be similar also at higher redshifts, as the behavior of the galaxy from K. Glazebrook et al. (2023) agrees well with the other galaxies. A larger simulation volume of the same resolution would however be needed to test this hypothesis with respect to the most extreme observed outlier quenched galaxy, which unfortunately is not available at the moment.

4. What Do They Become—The Multiple Pathways of Quenched Galaxies into the Future

As we have shown our simulated quenched galaxies to have similar properties as the observed quenched galaxies at high redshifts, we will now study their evolution forward in time to see if they stay quenched or rekindle their star formation. In the following we consider the evolution of the sample of galaxies, both quenched and star forming. As the simulation only evolved in high resolution down to $z \approx 2$, we can only trace the individual galaxy properties down to this redshift, but the overall properties can be followed in lower resolution down to $z = 0$.

4.1. Evolution to Redshift of z = 2

For the six most massive galaxies Figure 9 shows their star formation histories down to $z = 2$, going from top to bottom in order of galaxy ID. For comparison, the dotted lines of the same color show the star formation histories of the same galaxies when observed at $z = 3.4$, as shown in Figure 7, with all dotted lines reaching zero star formation before $z = 3.4$.

We find that for three of the central galaxies (ID16396 in pink, ID18258 in salmon, and ID22007 in yellow) there is practically no new stellar mass present at $z = 2$, neither accreted nor formed. That is to say they remain quenched down to $z = 2$. However, the fourth central quenched galaxy (ID20633 in orange) gained stellar mass, as there are more stars present with formation times $z_{\rm form} > 3.4$ compared to what was present in the main progenitor (dotted line). It is however not clear from this figure if the galaxy itself has rejuvenated or if it has only accreted matter. Nevertheless, while the largest peak of star formation for this galaxy before quenching produced about 20% of its stars as shown in Figure 7, the contribution of this peak only account for about 10%–12% with respect to the stellar mass of that galaxy at $z = 2$ as shown in Figure 9.

The first of the two satellites (ID4180 in black) eventually merges with its central, which is still actively forming stars, thereby significantly increasing its total stellar mass (hence the noticeable deviation to the dotted line also for $z_{\rm form} > 3.4$). At $z = 2$ the resulting galaxy is actively forming stars. However, this quenched galaxy was not rejuvenated but rather was the smaller member in a merger event and not the main progenitor of the resulting galaxy at $z = 2$. Interestingly, the galaxy that has consumed our quenched galaxy shows a star formation

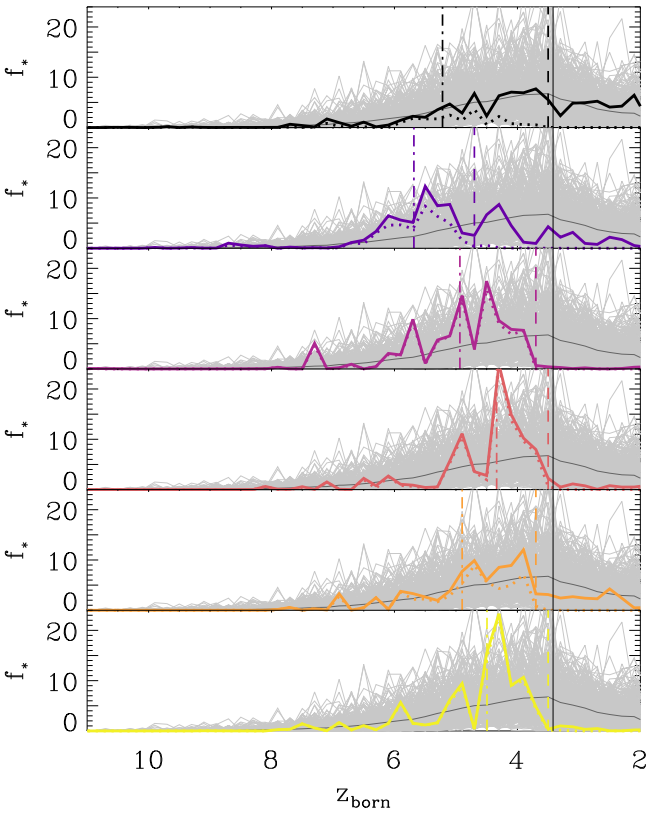

Figure 9. The fraction of stars as a percentage within the galaxy at $z = 2$ as a function of their formation redshift for each of the six most massive quenched galaxies (plotted in order of their IDs from top to bottom, ID4180, ID5058, ID16396, ID18258, ID20633, and ID22007). Plotted as colored dotted lines are the fractions at $z = 3.4$ when the galaxies are identified as quenched, as shown in Figure 7, rescaled to the total stellar mass at $z = 2$. The light gray lines show the formation histories of all galaxies with $M_* > 5 \times 10^{10}\ M_\odot$, with their mean in dark gray. The black vertical line denotes $z = 3.4$, with the colored vertical lines denoting $z_{\rm form}$ (dashed–dotted) and $z_{\rm quench}$ (dashed) when observed at $z = 3.4$.

history very similar to the main star formation history of all galaxies above $M_* > 5 \times 10^{10}\ M_\odot$ shown as gray line.

Finally, galaxy ID5058 (lilac) first merges with its central, and thus shows very similar behavior to ID4180 for $z_{\rm form} > 3.4$. Toward $z = 2$, however, the newly formed galaxy shows very little ongoing star formation, in stark contrast to galaxy ID4180. This is because after merging with its central, ID5058 then falls onto an even larger nearby galaxy group becoming a satellite again at $z = 2$. Here, the second galaxy also experiences quenching after it has consumed our quenched galaxy; this time, however, the quenching is a slow process as it is due to the new host's environment. It is the only case of environmental quenching that we found in our sample of quiescent galaxies at high redshifts.

Compared to the mean of the total sample of galaxies plotted in gray, the three which remain fully quenched naturally deviate most strongly toward earlier formation times. Interestingly, the two satellites which merge however show largely different behavior from one another, with ID4180 even exceeding the total sample's average fraction of stars formed at later times $z \approx 2$, while ID5058 suffers a second quenching event.

To see how other properties of the quenched galaxies evolve with time compared to similar galaxies, we consider the broader sample of the (II) mass cut. We reduce the sample to galaxies which are centrals at $z = 4.2$ and remain centrals until $z = 2$ to avoid including galaxies which may have quenched environmentally as opposed to internally. This results in 817 nonquenched and 22 quenched centrals, with their evolution of galactic properties shown in Figure 10.

The top left panel depicts the star formation rate of the sample. We find that the quenched galaxies all spike in their star formation rate in either of the two snapshots ($z = 4.2$ or $z = 5.3$) immediately before being quenched by $z = 3.4$. All but one exception reach star formation rates in excess of the median of nonquenched centrals (sand color line), with half exceeding the median by more than 1σ at either $z = 4.2$ or $z = 5.3$ (gray shaded area).

It is interesting to note here that the nonquenched sample of galaxies already more massive than $M_* > 3 \times 10^{10}\ M_\odot$ (sand line and gray shade) at $z = 3.4$ also have a strong drop in star formation rate toward $z = 2$, with the peak of its median at $z = 4.2$. This drop is much stronger than the slight decline found if all centrals with $M_* > 3 \times 10^{10}\ M_\odot$ at a given redshift are included, as shown by the black lines, which include also those which only recently rose above the stellar mass cut (median black dashed–dotted line, 1σ bounds given by the black dashed line). Consequently, if one were to observe all central galaxies at $z = 2$ those which have been massive centrals since $z = 4.2$ (around 2 Gyr) will generally have lower star formation rates. This also indicates that those galaxies that newly cross the mass threshold are still evolving due to ongoing star formation more strongly than those galaxies that have already formed stars early on.

The excess in star formation rate at early times correspondingly leads to the quenched galaxies lying at the higher end of stellar mass at $z > 4$, as can be seen in the top right panel of Figure 10. All but two of the 22 quenched centrals lie above the median stellar mass at $z = 4.2$ (sand color line). As all galaxies (quenched and nonquenched) are selected based on their stellar mass at $z = 3.4$ this means that the quenched galaxies generally formed their stellar mass earlier compared to similar galaxies. Following their evolution forward in time most remain quenched, forming (or accreting) little to no additional stellar mass over a time of around $t \approx 1.5$ Gyr. However, there are a few which gain sufficient amounts of new stars to reach the median of the total sample.

Interestingly, the total mass of the galaxies dips below the median for most quenched centrals at $z = 3.4$ (lower left panel of Figure 10). This is largely due to the significant ejection of gas which occurs during quenching (lower right panel of Figure 10). The gas is then replenished less quickly compared to the accretion of dark matter, resulting in the descendants at $z = 2$ of quenched centrals having average to slightly reduced total masses but significantly less gas and stellar mass. This means that the reduction in baryon fraction caused by the quenching process as described by K25 remains in place for most cases up to a time of 1.5 Gyr.

As we saw in the top left panel of Figure 10, the quenched centrals do not necessarily remain quenched. To define then whether a quenched galaxy has rejuvenated at some point after $z = 3.4$, we must consider what we mean by rejuvenation. It is for example possible that the quenched galaxy merges with a larger other galaxy which has ongoing star formation, as noted earlier for the cases of ID4180 and ID5058.

We begin first by considering the sample at $z = 2$, simply asking whether the quenched galaxies' descendants have rekindled their star formation to become normal main-sequence

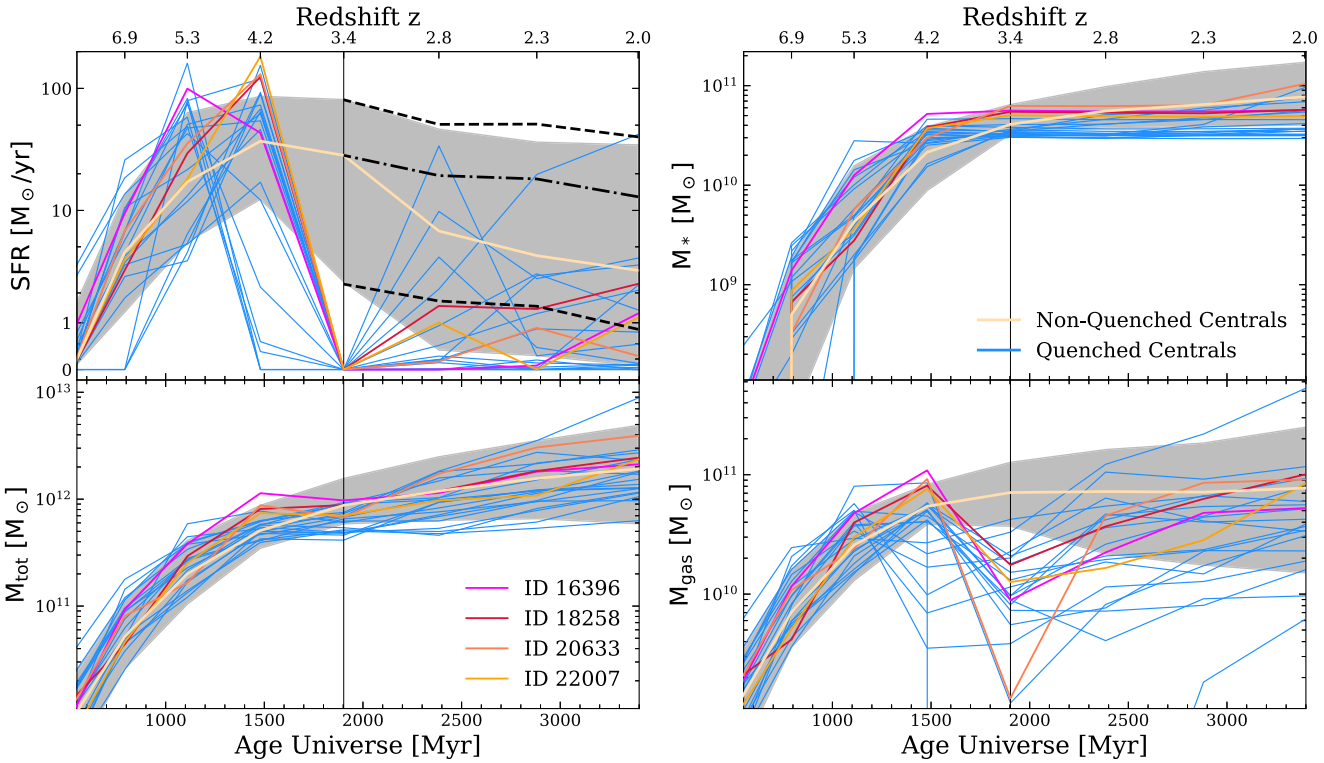

Figure 10. Redshift evolution of the star formation rate (upper left), stellar mass (upper right), the total mass (lower left), and gas mass (lower right) of centrals within the (II) mass cut, which remain centrals down to $z = 2$. For the 817 nonquenched galaxies the median is shown as sand color line, with 1σ as gray shaded. The individual evolutionary tracks of the 22 quenched galaxies are in blue, with the four most massive main galaxies at $z = 3.4$ as colored lines as in Figure 9. For the star formation rate the y-axis is scaled with $a$sinh. The black dash dotted line shows the mean SFR of all centrals (also including galaxies which fulfilled the mass cut only after $z = 3.4$), with the dashed black lines showing the 1σ range of this larger sample.

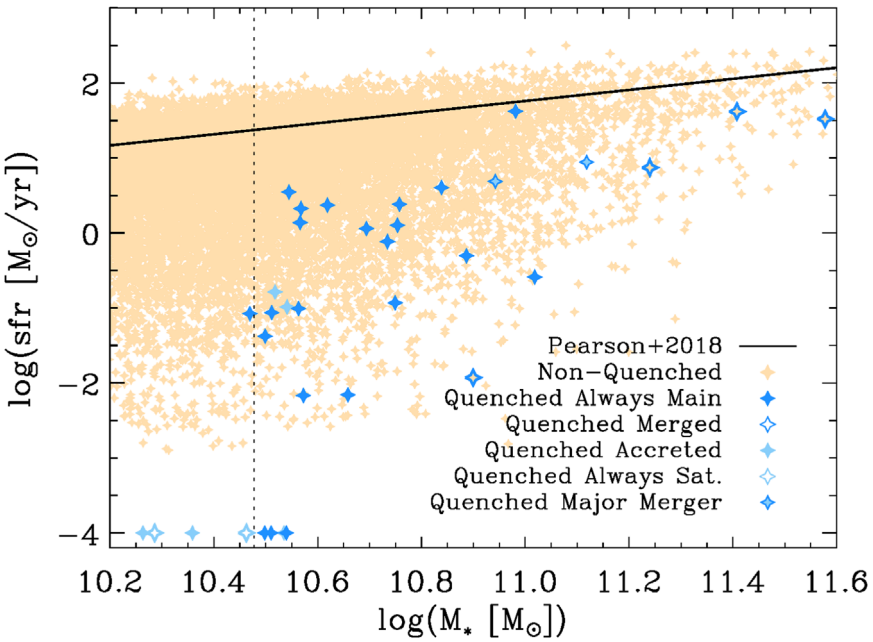

Figure 11. Star formation rate vs. stellar mass at $z = 2$ of the descendants of our sample of galaxies with mass cut (II), with the observed main sequence from W. J. Pearson et al. (2018) shown as a black line. Tan symbols are galaxies which were forming stars at $z = 3.4$, while blue symbols were quenched. We differentiate the second group into five subgroups, depending on their merger history postquenching.

galaxies. Figure 11 shows the star-forming main sequence at $z = 2$, with the blue stars being the traced descendants of the quenched galaxies and sand color points being all nonquenched galaxies (not only traced galaxies).

The quenched galaxies are split into five groups. First, those which were a satellite at the time of quenching at $z = 3.4$ and have remained a satellite down to $z = 2$ ("always sat"). Second, those which were centrals at $z = 3.4$ but were

accreted onto another larger halo but have not yet merged ("accreted"). Third, quenched galaxies which merged with another more massive structure, where the original quenched galaxy cannot be separated anymore ("merged"). Fourth, there are two cases where at the time of quenching the galaxy is closely interacting with another galaxy of comparable mass, and merges by $z = 2$ ("major merger"). Finally, those which remained centrals without ever merging with a larger galaxy ("always main").

Group one contains three galaxies (open light blue symbols). They all remain fully quenched, and the hot halo of their host galaxies (two of which become groups by $z = 2$) is thus efficient enough to suppress any rejuvenation of the star formation within the massive quenched galaxies already at $z > 2$. They also experience stripping, as their mass now is below our original stellar mass cut of $M_* = 3 \times 10^{10}\ M_\odot$, as marked by the dashed black line.

There are five quenched galaxies which are accreted onto other structures postquenching (filled light blue symbols). Their star formation rates are very low, with two fully quenched. However, unlike the "always sats," they are not entirely shutdown with three retaining very low residual star formation that they rekindled prior to infall in the more massive structure. Here, we see environmental quenching at work as these galaxies slowly loose their star formation abilities. They highlight that even for how massive the quenched galaxies are at $z = 3.4$, they do not necessarily remain the locally dominant node.

Four quenched galaxies merge (open dark blue symbols) with a more massive system to become a central by $z = 2$ (including ID4180). They contribute between one-tenth and one-third of the stellar mass at $z = 2$, and the descendant galaxy has high mass and star-forming activity. These are curious cases then where a quiescent galaxy is assembled onto a more massive star-forming galaxy, and the star formation is not quenched, opposite to the common pathway found at low redshift. Such remnant galaxies have extensive stellar bulges and are closer to S0 galaxies than typical disk galaxies.

Then we have two galaxies undergoing a major merger around the time of quenching (two-color symbols), one of which is ID5058. Both show a large growth in stellar mass and high star-forming activity, being very comparable to the behavior seen for the "merged" category. It follows that so long as the galaxy with which the quenched one merges is of equal or greater mass, the odds are it will become a "normal" sub-main-sequence galaxy.

The final group contains the 22 quenched centrals which remained centrals and never merged with any larger galaxy down to $z = 2$ (filled dark blue symbols). They represent the largest group, as well as the one with the most scatter in resulting star formation rates. These are the ones which we are most interested in for considering how many galaxies can rejuvenate from internal quenching through gradual feeding from the cosmic web.

Of these 22, we find a few which lie near the main sequence, with one in particular fully rejuvenating to lie on the relation. The majority lie at middling to low star formation rates, while three are still fully quenched. None have grown to stellar masses $M_* > 1 \times 10^{11}\ M_\odot$, with about half growing by less than 10%. Nonetheless, we find that star formation is not permanently shut off even for central galaxies which undergo violent quenching, eject their gas, and which subsequently have a large supermassive black hole at their core. These are not rejuvenated via major mergers bringing in significant gas, or by merging themselves with a more massive star-forming galaxy, but rather through accretion of gas from the cosmic web, and we will study this process in more detail in the following.

4.2. Rejuvenation

We differentiate between stars formed in other galaxies and are then accreted versus those which are formed within the galaxy itself, so in situ. To consider a newly formed star as in situ made, we require the progenitor gas particle to be within the virial radius of the central galaxy, and the resulting star to be bound to the central immediately afterwards. This gives four categories of stars in a given galaxy at $z = 2$: the initial old component which was in the galaxy at $z = 3.4$ ("old, in halo"); old stars which were formed elsewhere and accreted sometime after $z = 3.4$ ("old, accreted"); and younger stars (formed after $z = 3.4$) either made in situ ("new, in situ") or accreted ("new, accreted").

In the left panel of Figure 12 we show the mass fraction of in situ formed younger stars, $M_{*,\mathrm{new,in-situ}}/M_{*,\mathrm{new}}$ as a function of the fraction of total stellar mass contained in younger stars, $M_{*,\mathrm{new}}/M_{*,\mathrm{all}}$ for central galaxies at $z = 2$ traced from $z = 3.4$. We find that galaxies which have formed a significant fraction of their final mass recently tend also to have formed most of that mass in situ. This is because high-redshift galaxies contain significant fractions of gas, such that any accretion event involving young stars will also involve bringing in a lot of gas, enabling in situ star formation. Consequently, there emerges a lower bound to the fraction of young stars made in situ with a slope of around one. Put another way, if x% of all stars in a traced galaxy at $z = 2$ are young (<1.5 Gyr old), then at least x% of these young stars were made in situ (though the range can go up to 100% made in situ for any given x).

For the quenched galaxies this trend is largely absent, as there are multiple quenched galaxies with many young stars but few of which are in situ made. This indicates that galaxies which have quenched previously are better at prohibiting rekindling of their own star formation even when they accrete significant amounts of new matter compared to other nonquenched galaxies.

However, we also find that prior quenching of a galaxy does not mean that it cannot rejuvenate. Indeed, there are six galaxies which postquenching end up making at least 4% of their total stellar mass in situ afterwards. Three of them simultaneously grow by more than 10% while making at least 40% of these new young stars in situ (which lie in the upper right quadrant). Nine exhibit some lesser degree of star-forming activity, with five in the upper left (few new stars but mostly made in situ) and four in the lower right (many new stars but few of them self-made), while seven remain effectively quenched (lower left). This means we find that around 30% rejuvenate, 40% rekindle some residual star-forming activity, and 30% remain quenched throughout.

The location in the $M_{*,\mathrm{new,in-situ}}/M_{*,\mathrm{new}}$–$M_{*,\mathrm{new}}/M_{*,\mathrm{all}}$ plane gives the integrated star-forming activity, but how does it compare to the instantaneous star formation rate? To see this we color the points by their perpendicular distance to the star-forming main sequence at $z = 2$ as given by W. J. Pearson et al. (2018), normalized from zero (on the main sequence, dark

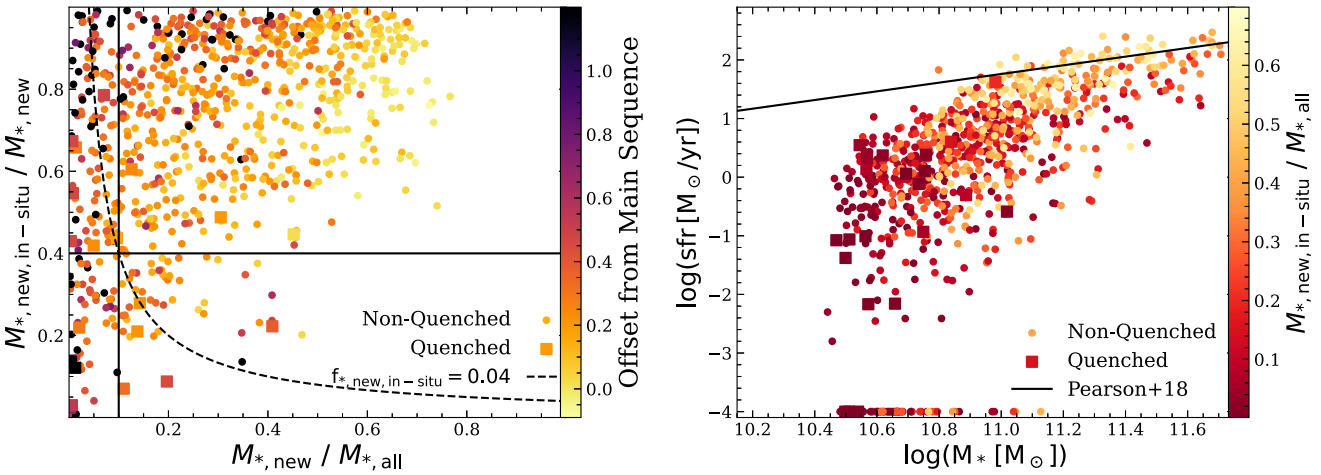

Figure 12. Left: fraction of young stars which are self-made vs. fraction of total stars which are young for traced centrals at $z = 2$, defined as nonquenched (dots) or quenched (square) based on the star formation rate at $z = 3.4$. Colored by a galaxy's perpendicular offset from the $z = 2$ main sequence, normalized between zero (lies on the main sequence, yellow) and one (farthest offset to the main sequence, purple), with starburst galaxies lying above the main sequence at <0 (yellow) and galaxies with star formation rate = 0 in black. The black dashed line denotes a fraction of young in situ stars $f_{*,\mathrm{new,in-situ}} = M_{*,\mathrm{new,in-situ}}/M_{*,\mathrm{all}} = 0.04$. Right: as Figure 11, but only galaxies which remained centrals from $z = 3.4$ to $z = 2$. Colored by the fraction of total stellar mass contained in young in situ stars.

yellow) to one (far below the main sequence, dark purple), with >1 being quenched (black) and <0 being star-bursting galaxies above the main sequence (yellow).

Interestingly, galaxies which end as quenched at $z = 2$ (black points) preferentially stick toward the perimeter, having either very little young stars (which lie far left) or having formed practically all younger stars in situ (which lie at the top). We interpret this as them quenching either through starvation caused by a lack of accretion (low $M_{*,\mathrm{new}}/M_{*,\mathrm{all}}$) or through the rapid starburst quenching mechanism described by K25, with a collapse of significant gas followed by a massive starburst (high $M_{*,\mathrm{new,in-situ}}/M_{*,\mathrm{new}}$) and combined stellar and AGN feedback, which quenches the star formation.

Generally, we find that when comparing galaxies which made a similar fraction of new stars in situ, those which show a higher instantaneous star formation rate (closer to the main sequence, more yellow) lie farther right (have a higher total fraction of younger stars). This also implies a higher total fraction of new in situ formation (an integrated quantity) based on the current star formation rate (an instantaneous quantity). To validate this we plot the star formation rate versus stellar mass in the right panel of Figure 12 and color by the total fraction of young in situ formed stars $M_{*,\mathrm{new,in-situ}}/M_{*,\mathrm{all}}$. We indeed find that galaxies lying closer to the main sequence show higher $M_{*,\mathrm{new,in-situ}}/M_{*,\mathrm{all}}$, though there is some scatter which warrants a closer look in the future.

Having seen that around 30% of the quenched galaxies rejuvenate we consider now where they make these new in situ stars, in particular when compared to galaxies which were not quenched at $z = 3.42$. We find in the left panel of Figure 13 that the new in situ stars in the six quenched descendants (blue color) which rejuvenated significantly ($M_{*,\mathrm{new,in-situ}}/M_{*,\mathrm{all}} >$ 0.4) lie at noticeably farther radii than in the nonquenched galaxies (sand color), indicating that the most central region does not experience significantly rekindled star formation once a galaxy has been quenched. This may also in part be caused by the comparatively more compact central bulges formed from the starburst which precedes the quenching (see also Figure 2), where at $z = 2$ the nonquenched sample have $\bar{r}_{1/2} \approx 3.1$ kpc while the quenched have $\bar{r}_{1/2} \approx 1.8$ kpc.

Taking the descendant of the quenched galaxy which has rejuvenated the most, galaxy ID25416, we plot the origin of its stellar component in the middle panel of Figure 13. The most central region within 1 $r_{1/2}$ is dominated by the original stars formed in the burst prior to quenching (red line). The stars which are formed in situ postquenching primarily reside between 1 $r_{1/2}$ and 3 $r_{1/2}$, where they also are the dominant component. Beyond around 5 $r_{1/2}$ the accreted components begin dominating, with comparable mass contained in younger versus older stars.

Finally we show the fraction of total stellar mass in young in situ stars as a function of their median radius for all individual galaxies. We find that galaxies with little recent in situ star formation also tend to have this formation occurring farther out. As the fraction of in situ formed stars increases they begin to dominate the total stellar mass budget, until eventually the stellar half-mass radius coincides with their median radius.

We then ask whether the degree of rejuvenation can be predicted from observables at the time of quenching already. Figure 14 shows the fraction of young in situ formed stars versus the surrounding gas within three virial radii, split by outflowing and inflowing components defined by $\boldsymbol{v} \cdot \boldsymbol{r} > 0$ and <0 (crosses and dots, respectively). The amount of mass is comparable in both components, and we find the outflowing gas to be generally hot (>$10^{5.4}$ K) while the inflowing gas is colder. We further see that a larger amount of inflowing cold gas (blue) results in a higher amount of rekindled in situ star formation, while there is no such correlation with the amount of outflow.

This dependence of rejuvenation on the inflowing gas mass indicates that it is the environment which ultimately determines the fate of high-z quenched galaxies as opposed to for example the mass of their AGN. Indeed, we find no correlation between the amount of rejuvenation $M_{*,\mathrm{new,in-situ}}/M_{*,\mathrm{all}}$ and the relative mass fraction of the black hole M_{BH}/M_* at $z = 3.4$ for the quenched galaxies. This mirrors the results by K25, where the

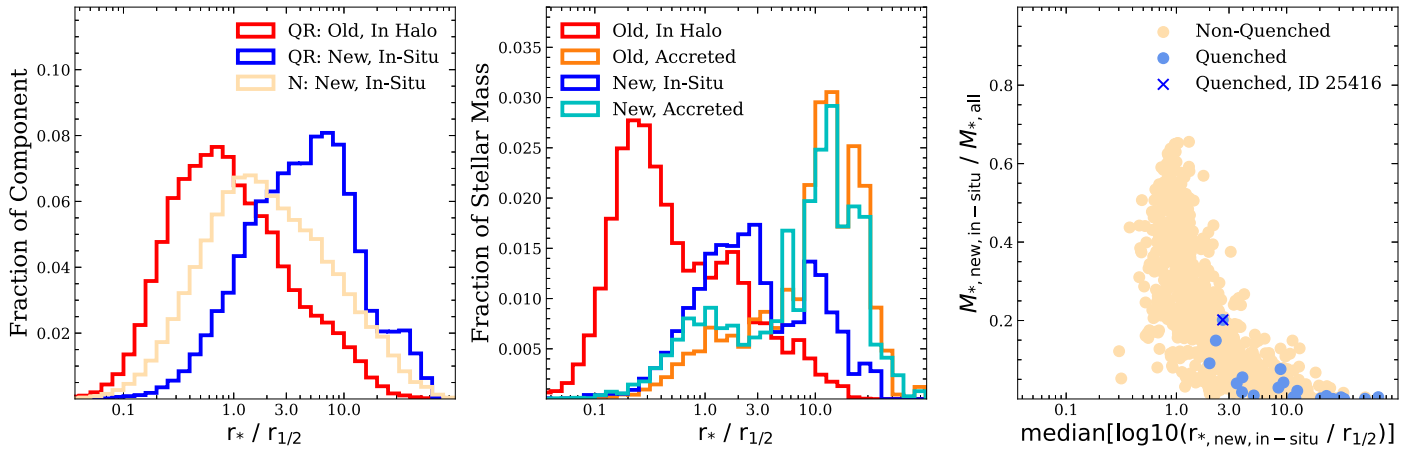

Figure 13. Left: radial distributions of the young in situ formed stars for the descendants of rejuvenated quenched (blue) and nonquenched (sand) galaxies at $z = 2$. The old component which was in the halo prior is also shown for the quenched descendants (red). Middle: the radial total mass fraction of different components (legend) for the quenched galaxy ID25416, which rejuvenates the strongest. Right: fraction of total stellar mass which is young and in situ made vs. its median radial position. All radii are given relative to the stellar half-mass radius.

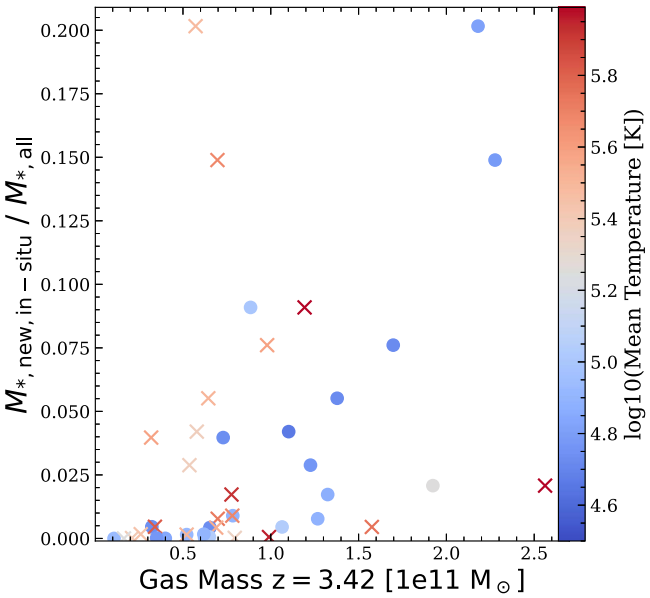

Figure 14. The fraction of stellar mass at $z = 2$ which was formed in situ postquenching (after $z = 3.4$) vs. the gas mass within three virial radii around the galaxy immediately following quenching (at $z = 3.4$). Gas is split into inflowing (dots) and outflowing components (crosses), and colored by the mean temperature.

long-term evolution of the star formation is most tightly correlated with the environment.

4.3. Descendant Galaxies at z = 0

Finally, we want to see where the quenched galaxies end up at present day. As the higher-resolution Box3 UHR simulation ran until $z \approx 2$, we match at the last snapshot the galaxies to their counterparts in the lower-resolution version of the same box, Box3 high-resolution run, which ran until $z = 0$. Note that exact matches are difficult in the case of satellites. However, as we care only about the final halo in which they end up in, it matters only that we can match the correct larger halo, which is generally possible.

The right panel of Figure 15 shows the histogram of the total mass of the host halo $M_{\rm all}$ at $z = 0$ for the descendants of the quenched (blue lines) and the nonquenched galaxies (tan lines). We find that the quenched galaxies generally end up in galaxy groups of a total mass around $M_{{\rm all},z=0} \approx 10^{13.5}\ M_\odot$. This is particularly true for the galaxies which were centrals at $z = 3.4$ (dashed blue line), with only three of 28 ending in galaxy clusters with $M_{{\rm all},z=0} \geqslant 10^{14}\ M_\odot$.

This means that on average they end in less massive halos compared to the total sample. The median mass of the final halo for nonquenched galaxies (sand lines) is $6.6 \times 10^{13}\ M_\odot$, while for quenched galaxies it is $4.4 \times 10^{13}\ M_\odot$. This difference is even more significant for centrals, with $5.8 \times 10^{13}\ M_\odot$ versus $3.8 \times 10^{13}\ M_\odot$, while for satellites the final halos are similar ($1.3 \times 10^{14}\ M_\odot$ versus $1.2 \times 10^{14}\ M_\odot$). That is to say we find that a massive central galaxy at $z = 3.4$ will on average end up in a halo of 50% higher mass at $z = 0$ if it is forming stars versus if it is fully quenched.

This imprint of the eventual halo mass is also present in the environment at higher redshifts. As an environmental tracer we define here d_5 as the radius of the sphere required to include five neighboring galaxies with total masses $M_{\rm all} \geqslant 10^{11}\ M_\odot$. The final halo mass at $z = 0$ is then plotted against this radius calculated at $z = 3.4$ in the left panel of Figure 15.

We find that there is a diffuse correlation between a more dense environment at $z = 3.4$ (lower d_5) and a higher final halo mass at $z = 0$. This is overall to be expected as R.-S. Remus et al. (2023) find that the environment is the best tracer for the $z = 0$ mass of protoclusters. What is striking, however, is that of the 28 quenched centrals (blue filled dots) 75% lie above the median separation of all galaxies (vertical black line), so lie in underdense environments.

This may mean that a specific type of environment is required to fully self-quench through combined stellar and AGN feedback. Indeed, it is reasonable to assume that denser environments are more proficient at replenishing lost gas. To remove enough gas to completely cease star formation requires so little gas accretion that the feedback can overpower the inflow. This idea is explored further in K25 and explains why

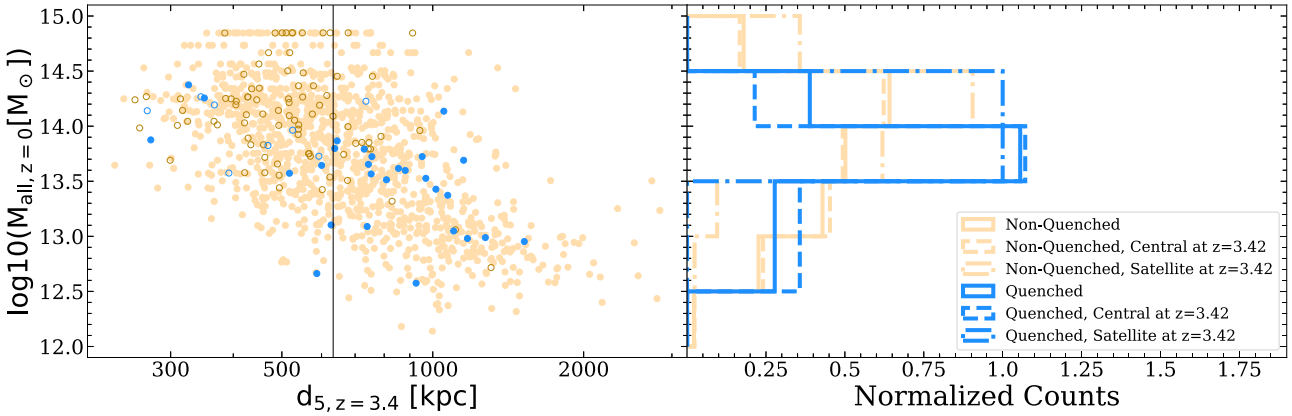

Figure 15. Left: total halo mass at $z = 0$ plotted against a tracer for the environment at $z = 3.4$, d_5 (in units of physical kpc), for quenched (blue) and nonquenched (sand) centrals (filled symbols) and satellites (open symbols), defined at $z = 3.4$. The median d_5 for all galaxies is given by the vertical black line. Right: binned total halo mass at $z = 0$.

here the quenched galaxies are found predominantly in underdense environments.

5. Summary and Conclusions

We studied quenched galaxies identified at $z = 3.4$ in the Magneticum Pathfinder large high-resolution Box3 UHR simulation and compared their properties to observations of quenched galaxies from JWST by T. Nanayakkara et al. (2022), F. Valentino et al. (2023), and A. C. Carnall et al. (2023), and also to pre-JWST observations of quenched number densities. We show that the Magneticum simulation can successfully reproduce similar quenched fractions for comparable stellar masses to those observed, albeit we cannot reproduce the most massive of the quenched galaxies as the box volume of the simulation is still too small to capture these biggest nodes. We also compared the observations and the Magneticum number densities to those of other simulations like IllustrisTNG, Eagle, Astrid, and Flares, which struggle to capture the quenched fractions at $z > 3.5$ as shown also by E. J. Weller et al. (2025). As discussed in more detail by K25, it is likely that these differences originate from differing implementations of the AGN feedback schemes. The Magneticum simulations used here differentiate between hot and cold gas accretion onto the black hole, allowing for increased accretion rates at higher redshifts while simultaneously dampening them at intermediate redshifts (L. K. Steinborn et al. 2015). By contrast, other models typically couple to the total gas reservoir, which may be underestimating variability in the black hole mass accretion and thus feedback, resulting in both fewer quenched galaxies at high redshifts and subsequently also less rejuvenation.

We find the quenched galaxies to be rather compact in size compared to nonquenched galaxies, in good agreement with recent observations by K. Ito et al. (2024) and A. C. Carnall et al. (2024), albeit being generally a bit larger than observed due to the limiting softening length of the simulation. Furthermore, the formation redshifts of the simulated quenched galaxies are in good agreement with the observed formation redshifts, with some reaching up to $z_{\rm form} \approx 6$, aside from the observation of a peculiar quenched galaxy reported by K. Glazebrook et al. (2023), which is older than any formation redshift we can produce here. However, our full simulation sample contains at least one galaxy that is quenched at about $z = 5$ and which has a formation redshift beyond $z = 8$ but which rejuvenated afterwards, as shown in the companion study to this work by K25.

All our quenched galaxies experience a fast period of star formation followed by a rapid decline that leads to quenching, resulting in similar quenching redshifts as observed. In fact, we find that the quenching redshifts and formation redshifts of the quenched galaxies are correlated, with galaxies with higher formation redshifts also having higher quenching redshifts. This is found for both simulations and observations to be the case, and the outlier quenched galaxy from the observed sample by K. Glazebrook et al. (2023) actually follows the same trend as the simulations predict if extrapolated to higher redshifts. This indicates that quenching at high redshifts proceeds in a like manner, consistently occurring on very short timescales after a massive star formation event, which is in agreement with what is discussed by K25.

We follow the quenched galaxies forward in time, and find that by $z = 2$, that is within 1.5 Gyr after being fully quenched, about 20% of the galaxies that are centrals at $z = 3.4$ are accreted onto a more massive structure by $z = 2$, and are either still satellites of that structure or have merged with the more massive central galaxy. Of the remaining 80% of quenched galaxies, 30% rejuvenate, 30% remain fully quenched, and 40% develop some residual star formation. Those galaxies that rejuvenate can even reach the star formation main sequence and appear at a later time to be normal star-forming galaxies.

For those quenched galaxies that rejuvenate, we find the star formation to primarily occur on the outskirts between 1 $r_{1/2}$ and 3 $r_{1/2}$, not reaching the central regions. This is different to the nonquenched comparison sample of galaxies that are already massive at $z = 3.4$, where star formation can still occur at the center even down to $z = 2$. Furthermore, we find that the amount of newly formed stars postquenching primarily correlates with the amount of cold gas that has been inflowing, while there is no correlation to the outflowing hot gas component, clearly showing that the rejuvenation only depends on new inflowing gas reaching the galaxy, independent of the mass of the AGN that drives the hot wind outwards.

Finally, we find that quenched galaxies at $z = 3.4$ tend to end up in less massive final halos at $z = 0$ compared to nonquenched massive galaxies at $z = 3.4$. This difference is negligible for galaxies that become satellites by $z = 2$, but significant for galaxies that stay centrals, with the final mass deviating on average by 50%. This is because whether a galaxy is star

forming or not at high redshift correlates with the environment, where we showed that quenched galaxies tend to lie in underdense regions. We conclude that the environment of a galaxy at high redshift is not only important for it being quenched as shown by K25, but that it also plays a crucial role for the future development of the quenched galaxies at low redshifts. Thus, we suggest that relics of galaxies quenched at high redshifts can best be found in low-mass group environments or isolated fields, albeit it might be possible for a high-redshift quenched galaxy to be accreted onto a cluster and still remain as a compact quenched galaxy. As the quenched galaxies at high redshifts are very compact, relics of such galaxies should also still be significantly more compact than other quenched galaxies of comparable mass at present day. Nevertheless, as some quenched galaxies also merge with other, still star-forming galaxies prior to $z = 2$, it is also possible to find contributions of the quenched galaxies distributed in other galaxies, however, detecting those might be extremely difficult.

Acknowledgments

We thank the anonymous referee for their helpful comments. We also would like to thank Klaus Dolag for inspiring discussions. This work was supported by the Deutsche Forschungsgemeinschaft (DFG; German Research Foundation) under Germany's Excellence Strategy—EXC-2094-390783311. L.C.K. acknowledges support by the DFG project No. 51635 5818. The Magneticum simulations were performed at the Leibniz-Rechenzentrum with CPU time assigned to the Project pr83li. We are especially grateful for the support by M. Petkova through the Computational Center for Particle and Astrophysics (C2PAP).

References

Adams, N. J., Conselice, C. J., Ferreira, L., et al. 2023, MNRAS, 518, 4755
Antwi-Danso, J., Papovich, C., Esdaile, J., et al. 2025, ApJ, 978, 90
Arrabal Haro, P., Dickinson, M., Finkelstein, S. L., et al. 2023, Natur, 622, 707
Beck, A. M., Murante, G., Arth, A., et al. 2016, MNRAS, 455, 2110
Bell, E. F., Naab, T., McIntosh, D. H., et al. 2006, ApJ, 640, 241
Bezanson, R., van Dokkum, P. G., Tal, T., et al. 2009, ApJ, 697, 1290
Bournaud, F., Jog, C. J., & Combes, F. 2007, A&A, 476, 1179
Carnall, A. C., Cullen, F., McLure, R. J., et al. 2024, MNRAS, 534, 325
Carnall, A. C., McLeod, D. J., McLure, R. J., et al. 2023, MNRAS, 520, 3974
Carnall, A. C., Walker, S., McLure, R. J., et al. 2020, MNRAS, 496, 695
Chabrier, G. 2003, PASP, 115, 763
Chauke, P., van der Wel, A., Pacifici, C., et al. 2019, ApJ, 877, 48
de Graaff, A., Setton, D. J., Brammer, G., et al. 2025, NatAs, 9, 280
Dolag, K., Borgani, S., Murante, G., & Springel, V. 2009, MNRAS, 399, 497
Dolag, K., Jubelgas, M., Springel, V., Borgani, S., & Rasia, E. 2004, ApJL, 606, L97
Dolag, K., Vazza, F., Brunetti, G., & Tormen, G. 2005, MNRAS, 364, 753
Donnert, J., Dolag, K., Brunetti, G., & Cassano, R. 2013, MNRAS, 429, 3564
Fabjan, D., Borgani, S., Tornatore, L., et al. 2010, MNRAS, 401, 1670
Forrest, B., Cooper, M. C., Muzzin, A., et al. 2024, ApJ, 977, 51
Franx, M., van Dokkum, P. G., Förster Schreiber, N. M., et al. 2008, ApJ, 688, 770
Fudamoto, Y., Inoue, A. K., & Sugahara, Y. 2022, ApJL, 938, L24
Fudamoto, Y., Oesch, P. A., Schouws, S., et al. 2021, Natur, 597, 489
Gaspari, M., Ruszkowski, M., & Oh, S. P. 2013, MNRAS, 432, 3401
Glazebrook, K., Nanayakkara, T., Schreiber, C., et al. 2023, Natur, 628, 277
Gould, K. M. L., Brammer, G., Valentino, F., et al. 2023, AJ, 165, 248
Haardt, F., & Madau, P. 2001, in Clusters of Galaxies and the High Redshift Universe Observed in X-Rays, Recent Results of XMM-Newton and Chandra, ed. D. M. Neumann & J. T. V. Tran, 64
Harikane, Y., Nakajima, K., Ouchi, M., et al. 2024, ApJ, 960, 56
Harikane, Y., Ouchi, M., Oguri, M., et al. 2023, ApJS, 265, 5
Hartley, A. I., Nelson, E. J., Suess, K. A., et al. 2023, MNRAS, 522, 3138
Hilz, M., Naab, T., Ostriker, J. P., et al. 2012, MNRAS, 425, 3119
Hirschmann, M., Dolag, K., Saro, A., et al. 2014, MNRAS, 442, 2304
Ito, K., Valentino, F., Brammer, G., et al. 2024, ApJ, 964, 192
Kakimoto, T., Tanaka, M., Onodera, M., et al. 2024, ApJ, 963, 49
Karademir, G. S., Remus, R.-S., Burkert, A., et al. 2019, MNRAS, 487, 318
Kimmig, L. C., Remus, R.-S., Seidel, B., et al. 2025, ApJ, 979, 15
Komatsu, E., Smith, K. M., Dunkley, J., et al. 2011, ApJS, 192, 18
Kurinchi-Vendhan, S., Farcy, M., Hirschmann, M., & Valentino, F. 2024, MNRAS, 534, 3974
Lange, R., Driver, S. P., Robotham, A. S. G., et al. 2015, MNRAS, 447, 2603
Lelli, F., Zhang, Z.-Y., Bisbas, T. G., et al. 2023, A&A, 672, A106
Long, A. S., Antwi-Danso, J., Lambrides, E. L., et al. 2024, ApJ, 970, 68
Martin-Navarro, I., Shankar, F., & Mezcua, M. 2022, MNRAS, 513, L10
Merlin, E., Fortuni, F., Torelli, M., et al. 2019, MNRAS, 490, 3309
Naab, T., Johansson, P. H., & Ostriker, J. P. 2009, ApJL, 699, L178
Nanayakkara, T., Glazebrook, K., Jacobs, C., et al. 2024, NatSR, 14, 3724
Nelson, E. J., Suess, K. A., Bezanson, R., et al. 2023, ApJL, 948, L18
Pearson, W. J., Wang, L., Hurley, P. D., et al. 2018, A&A, 615, A146
Remus, R.-S., Dolag, K., & Dannerbauer, H. 2023, ApJ, 950, 191
Remus, R.-S., Dolag, K., Naab, T., et al. 2017, MNRAS, 464, 3742
Rizzo, F., Roman-Oliveira, F., Fraternali, F., et al. 2023, A&A, 679, 129
Roman-Oliveira, F., Fraternali, F., & Rizzo, F. 2023, MNRAS, 521, 1045
Salmon, B., Papovich, C., Finkelstein, S. L., et al. 2015, ApJ, 799, 183
Schreiber, C., Glazebrook, K., Nanayakkara, T., et al. 2018, A&A, 618, A85
Schulze, F., Remus, R.-S., Dolag, K., et al. 2018, MNRAS, 480, 4636
Shahidi, A., Mobasher, B., Nayyeri, H., et al. 2020, ApJ, 897, 44
Springel, V. 2005, MNRAS, 364, 1105
Springel, V., & Hernquist, L. 2003, MNRAS, 339, 289
Springel, V., White, S. D. M., Jenkins, A., et al. 2005, Natur, 435, 629
Springel, V., White, S. D. M., Tormen, G., & Kauffmann, G. 2001, MNRAS, 328, 726
Steinborn, L. K., Dolag, K., Hirschmann, M., Prieto, M. A., & Remus, R.-S. 2015, MNRAS, 448, 1504
Straatman, C. M. S., Labbé, I., Spitler, L. R., et al. 2014, ApJL, 783, L14
Tanaka, T. S., Shimasaku, K., Tacchella, S., et al. 2024, PASJ, 76, 1
Teklu, A. F., Remus, R.-S., Dolag, K., et al. 2015, ApJ, 812, 29
Tornatore, L., Borgani, S., Dolag, K., & Matteucci, F. 2007, MNRAS, 382, 1050
Tornatore, L., Borgani, S., Matteucci, F., Recchi, S., & Tozzi, P. 2004, MNRAS, 349, L19
Tsukui, T., & Iguchi, S. 2021, Sci, 372, 1201
Tsukui, T., Wisnioski, E., Krumholz, M. R., & Battisti, A. 2023, MNRAS, 523, 4654
Urbano Stawinski, S. M., Cooper, M. C., Forrest, B., et al. 2024, OJAp, 7, 46
Valentino, F., Brammer, G., Gould, K. M. L., et al. 2023, ApJ, 947, 20
van der Wel, A., Franx, M., van Dokkum, P. G., et al. 2014, ApJ, 788, 28
Weaver, J. R., Davidzon, I., Toft, S., et al. 2023, A&A, 677, A184
Weller, E. J., Pacucci, F., Ni, Y., Hernquist, L., & Park, M. 2025, ApJ, 979, 181
Wiersma, R. P. C., Schaye, J., & Smith, B. D. 2009, MNRAS, 393, 99
Yi, S. K., Yoon, S. J., Kaviraj, S., et al. 2005, ApJL, 619, L111
Zhang, J., Li, Y., Leja, J., et al. 2023, ApJ, 952, 6